AD612498

RADC-TR-64-568

INVESTIGATION OF GAS IONIZATION PHENOMENON AT OPTICAL AND IR FREQUENCIES

COPY 2 OF 3
HARD COPY $. 3.00
MICROFICHE $. 0.75
88 p

TECHNICAL REPORT NO. RADC-TR-64-568
February 1965

DDC
MAR 22 1965
DDC-IRA B

Instrumentation Branch
Rome Air Development Center
Research and Technology Division
Air Force Systems Command
Griffiss Air Force Base, New York

ARCHIVE COPY

No DDC limit

INVESTIGATION OF GAS IONIZATION PHENOMENON AT OPTICAL AND IR FREQUENCIES

AIR FORCE, GAFB, N.Y., 19 MAR 68-104

FOREWORD

This second interim technical report was prepared for Rome Air Development Center under Contract AF30(602)-3332 by the Surface Division, Defense and Space Center, Westinghouse Electric Corporation, Baltimore, Maryland.

The project engineer was Vincent Dovydaitis, Jr. The system number is 760B, the project number is 5561 and the task number is 556106.

This technical report has been reviewed and is approved.

Approved: Vincent Dovydaitis Jr.
VINCENT DOVYDAITIS, JR.
Contract Engineer

Approved:
JOSEPH FALLIK
Ch, Space Surveillance and
Instrumentation Branch
Surveillance & Control Division

ABSTRACT

The status of the current work on ruby laser induced gas ionization is reported. Experimental measurements of the focused spot diameter, breakdown emission, ionization times and nonattenuation ionization are presented. The theoretical study results obtained to date in the areas of nonlinear ionization initiation and the extension of the microwave breakdown theory are discussed.

TABLE OF CONTENTS

LIST OF ILLUSTRATIONS

I. INTRODUCTION

A. PURPOSE

This is the second technical documentary report for contract number AF30(602)3332 under the sponsorship of the Rome Air Development Center. The period of work covered is from 11 August 1964 to 11 December 1964. The status of the current work, results obtained to date, and future work to be performed are discussed.

This contract is for the investigation and study of the breakdown (ionization) mechanisms of gases at optical/infrared frequencies. The investigation includes both theoretical and experimental research, using lasers, into the power densities required to ionize air between about 1000 pounds per square inch and 10^{-6} millimeters of mercury, and the mechanisms responsible for such ionization. Approaches employed account for mechanisms of breakdown of several pure gases and gas mixtures chosen by the researchers, as well as air. Ionization is determined as a function of time, gas ionization potentials, pressure, frequency of incident beam, presence of outside agents (container walls, surfaces, ionizing radiation), and other pertinent parameters.

B. PROGRAM

As shown in the gas ionization program flow diagram, figure I-1, two parallel programs were conducted, one for experiments and the other for theoretical studies. A continuous interchange exists between the experimental and study areas, permitting theory to help guide the experimental approach and the experimental results to help develop and confirm the theoretical descriptions.

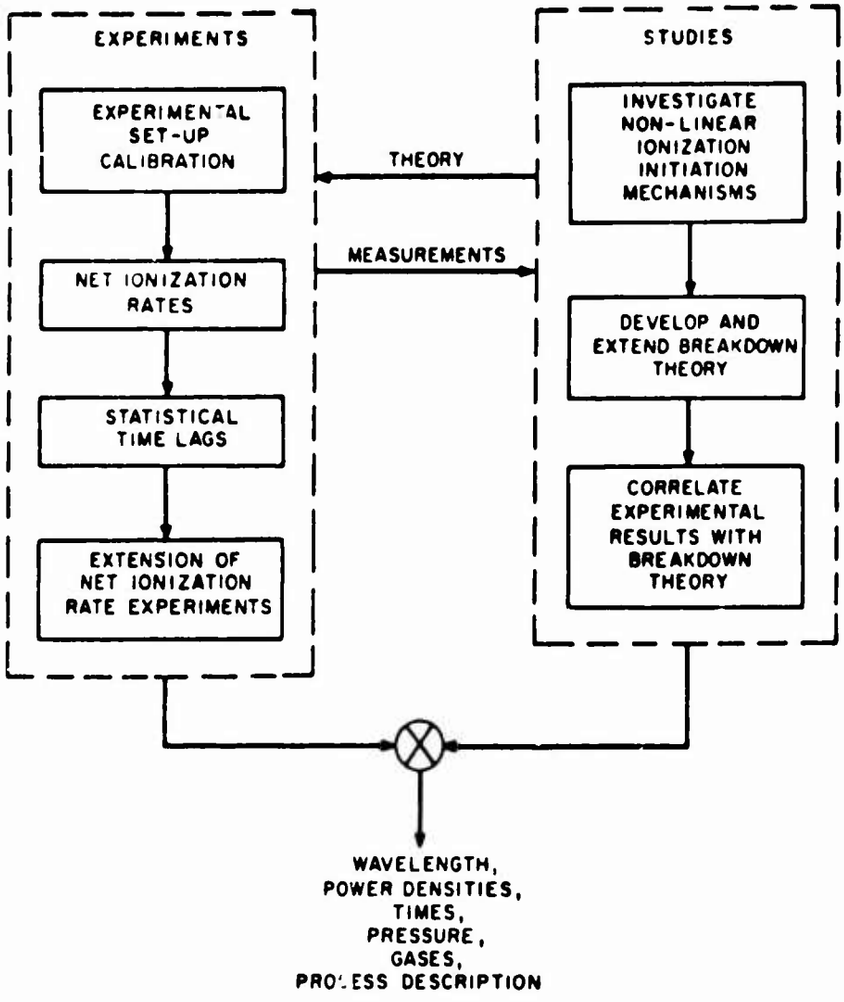

Figure I-1. Gas Ionization Program

Basically, two types of experiments are to be performed: (1) the measurement of the net ionization rates and (2) the statistical time lags. The critical nature of the experiments required first an experimental setup calibration. For program expediency, the net ionization rates experiments are divided into two phases. The first phase determines these rates for a few representative gases at selected gas pressures and allows the basic mechanism to be isolated early in the program, thus aiding the theoretical analysis. The second phase extends these rate measurements for the full range of pressures and gases.

The first set of net ionization rate experiments is to determine the rate of ionization buildup once the process is initiated. If it is exponential, the mechanism can be characterized as an avalanche-type process similar to the well-known microwave breakdown. However, if the buildup is linear, the ionization rate must depend on a different type of mechanism. At the high power densities required for optical breakdown very high field strengths exist. These fields may be sufficient to induce direct ionization of the gas molecules by photons, rather than depending upon the collision mechanism that accounts for microwave breakdown.

The statistical time lag experiments are to determine how the ionization process is initiated. The avalanche ionization buildup, which depends upon initial ions being present within the volume subject to the electric field, furnishes the electrons that start the ionization process. The random nature of the ion distribution in the gases should cause a statistical time lag in the ionization initiation for those mechanisms that depend upon their presence. If the intense optical field can directly ionize the gas molecules, a much less statistical effect in the ionization initiation will be observed.

The theoretical studies are divided into three areas. Two of the study areas began in the early part of the program (i.e., the investigation of the non-linear ionization initiation mechanisms and the development and extension of the breakdown theory). The third study area correlates the experimental results with breakdown theory. If disagreement is evident, the theory will be modified to agree with the experiments to obtain a quantitative description of the breakdown mechanisms.

C. STATUS

At the end of this reporting period, measurements of the focused spot diameter for several lenses were completed. Data on breakdown emission from Argon during and after laser irradiation were obtained. Ionization times versus electric field for different focal spot diameters were also recorded for Argon. Breakdown measurements were obtained for helium. Charge collection measurements were made at very low air pressures to try to determine the ionization build-up process. Experiments have begun using a variable pressure test cell.

The theoretical studies considered both the non-linear ionization initiation mechanisms and the extension of the microwave breakdown theory. Attempts to find useful expressions for the rates of non-linear ionization have continued but without success. Investigation of the rate of photon absorption in free-free transitions has continued.

II. SUMMARY AND CONCLUSIONS

A. PROCESS DESCRIPTION

The theoretical and experimental data available at present are consistent with the following sequence of events. It appears that the growth of ionization begins with the production of a small number of electron-ion pairs from impurities or from the main gas by a non-linear or multi-photon process. The electron and ion density then begins to grow by an electron multiplication, or avalanche process, which probably involves multiphoton photoionization of excited atoms. When a very small fraction of the gas is ionized (e.g., less than one part in 10^8 at atmospheric pressure), space charge effects become large enough to reduce the electron loss and increase the rate of electron multiplication. Finally, when the gas is nearly completely ionized, the absorption of laser energy in electron-neutral collisions is augmented by absorption in electron-ion collisions and in some cases by absorption by excited atoms. This final stage produces the observed absorption of the laser beam and most of the light output.

B. EXPERIMENTAL WORK

The process of gas ionization shows a threshold dependence upon the intensity distribution in the laser beam. Since significant changes in the intensity distribution can cause significant changes in spot size, care must be taken to monitor these variations. Secondly, spot size for short focal length lenses cannot be determined from a knowledge of beam divergence, thus making accurate measurements of spot size an important parameter to define experimentally. Reducing the spot size by use of a 5.08 cm focal length lens lowered the time of breakdown for a given field strength as compared to that for a 3.3 cm lens.

Results of the work done in helium indicate that the spectral emission of the plasma differs for the various gases. The easily ionizable mercury vapor had no detectable effect on the breakdown time in helium.

3. THEORETICAL WORK

Evidence is presented that the absorption of relatively high energy photons in free-free transitions may in some cases lead to small ($\sim$ 30%) but possibly significant deviations in the rate of growth of an electron avalanche from that predicted by an appropriate extension of the microwave theory, i.e., the continuous form of the Boltzmann equation. This evidence is obtained by solving the difference form of the Boltzmann equation in both the steady state and time dependent cases for various simple models of the electron-atom or electron-ion collision processes. However, since direction and magnitude of the deviation depend upon the model used and since several important effects are not included, further comparisons of the two theories are desirable.

Additional calculations of the excitation, ionization, and diffusion coefficients are presented and used to compute avalanche growth times and approximate curves of the laser intensity required for breakdown as a function of gas density. In general the agreement between theory and experiment is within a factor of two in laser intensity or 40% in laser electric field intensity. There are, however, systematic deviations between theory and experiment which should be explored further.

III. GAS IONIZATION EXPERIMENTS*

A. VARIATIONS IN THRESHOLD MEASUREMENTS

The measurements of the time of breakdown in argon as determined from the time of attenuation of the transmitted laser light versus total energy were shown in Figures III-9, III-10, and III-11 of the first interim report. In those measurements a large difference in the threshold of breakdown (lowest energy producing attenuation) existed between Figures III-9 and III-10 & 11. Differences in the data due to two separate gas cells were ruled out by interchanging the cell used to produce the data shown in Figure III-9 and observing data similar to that shown in III-10 and III-11. Replacement of the focusing lens was then thought to have caused the discrepancy. Further analysis of the intensity distribution showed the real cause of the threshold change. An analysis of the intensity distribution had shown that the effective beam divergence varied between 2.1 and 2.6 milliradians. At that time it was thought that this beam divergence was characteristic of the system at all times. The analysis of the beam divergence during later experimentation revealed that the angle of divergence was then about 0.8 milliradians. These changes in beam divergence were observed during subsequent experiments and measured to vary by as much as several milliradians. The changes seemed to accompany the replacement of the xenon flashlamp used to excite the ruby. The variation in the angle of divergence during the life of any one lamp seemed to be about 25%. As yet there does not seem to be a noticeable correlation between these smaller variations in divergence angle and the small variation in time of breakdown versus total energy.

*This work was performed by R. W. Waynant

B. MEASUREMENT OF FOCUSED SPOT SIZE

The measurement of the focused spot size was underway at the time of the first interim report. The measuring technique was outlined in that document. The data for several lenses has since been analyzed and will be reported here. Graphs showing the diameter of the spot as a function of distance from the center of the lens are shown in Figures III-1, III-2, and III-3. In the case of the lenses with 12.7 cm and 5.08 cm focal lengths a glass plate was inserted between the lens and the photographic film in order to simulate the conditions encountered with the gas cell. This probably accounts for the fact that the smallest measured diameter was found at distances greater than the focal length stated by the manufacturer. Since the 3.3 cm focal length lens will go into the stainless steel test cell, the spot size for two of these lenses were measured. In all cases, the measured diameter of the spot size was larger than the diameter calculated from angular divergence data. This indicates that spherical abberation in the lens plays an important part in spot size determinations.

The measurements of spot size for the 12.7 cm lens show considerable variation of the spot diameter versus distance from the lens. These variations as shown in the plot have not been corrected for changes in the intensity distributions, but such correction seems only to exagerate the variations. This would perhaps suggest that an axial variation in the focused region is being observed. These variations were not so evident in the plots for the 5.08 cm and 3.3 cm focal length lenses.

C. MEASUREMENT OF BREAKDOWN EMISSION FROM ARGON

Guided by theoretical calculations which predicted short excited state lifetimes during laser irradiation, work was done to examine the emission from the ionized region of the gas. In this work a monochromator was utilized to

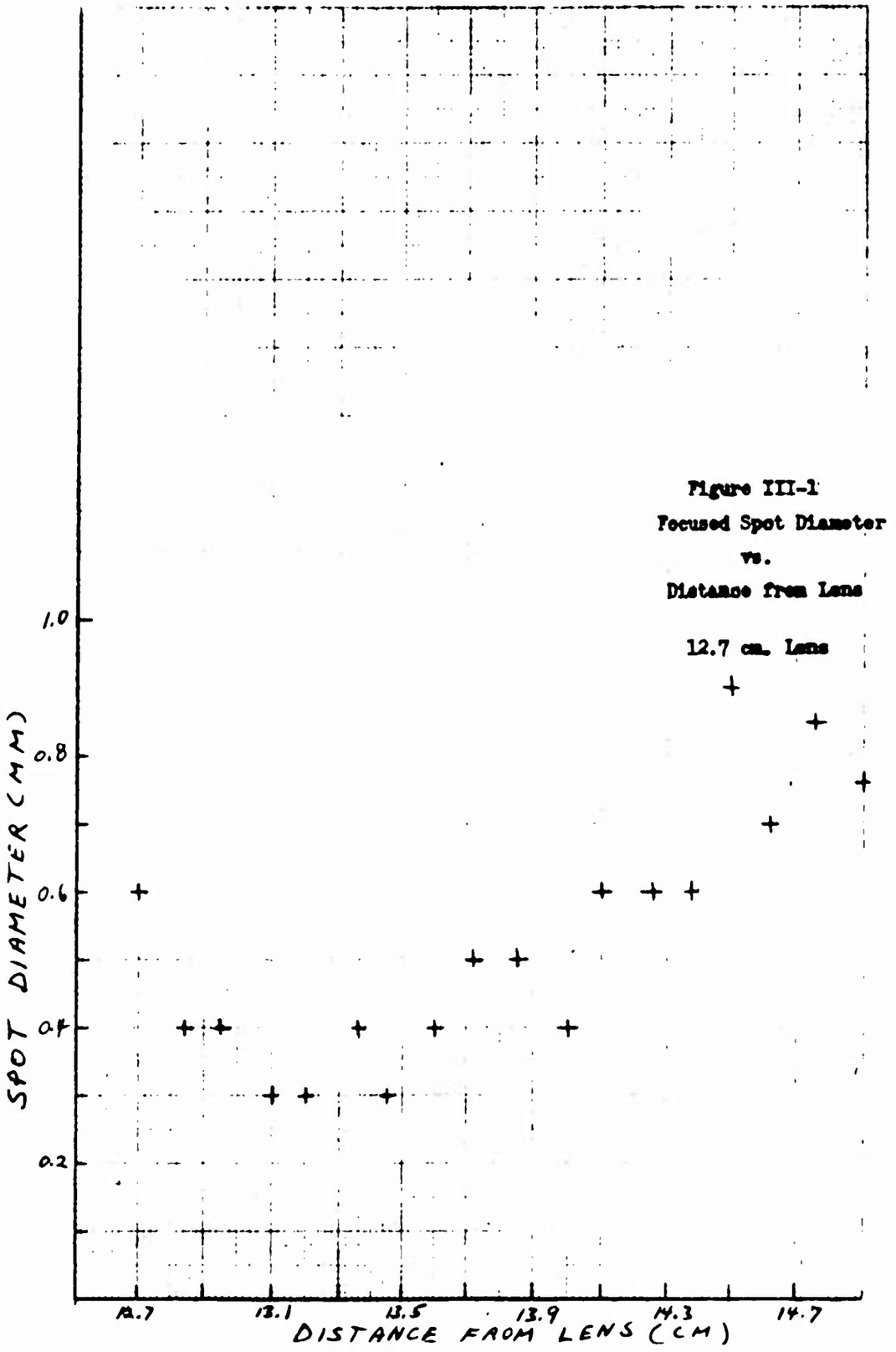

Figure III-1
Focused Spot Diameter
vs.
Distance from Lens

12.7 cm. Lens

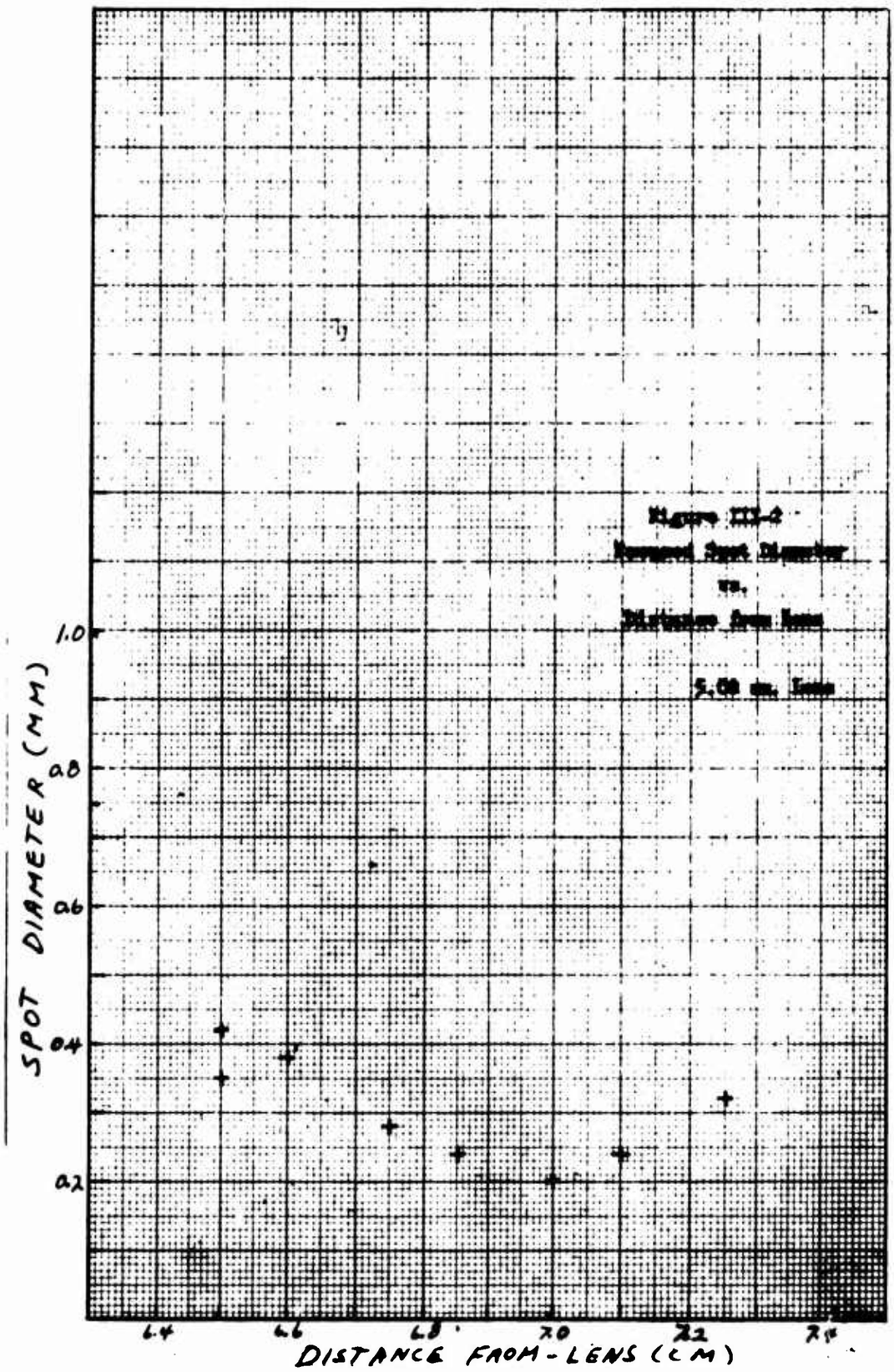

Figure III-4
Measured Spot Diameter
vs.
Distance from Lens
5.08 cm. Lens

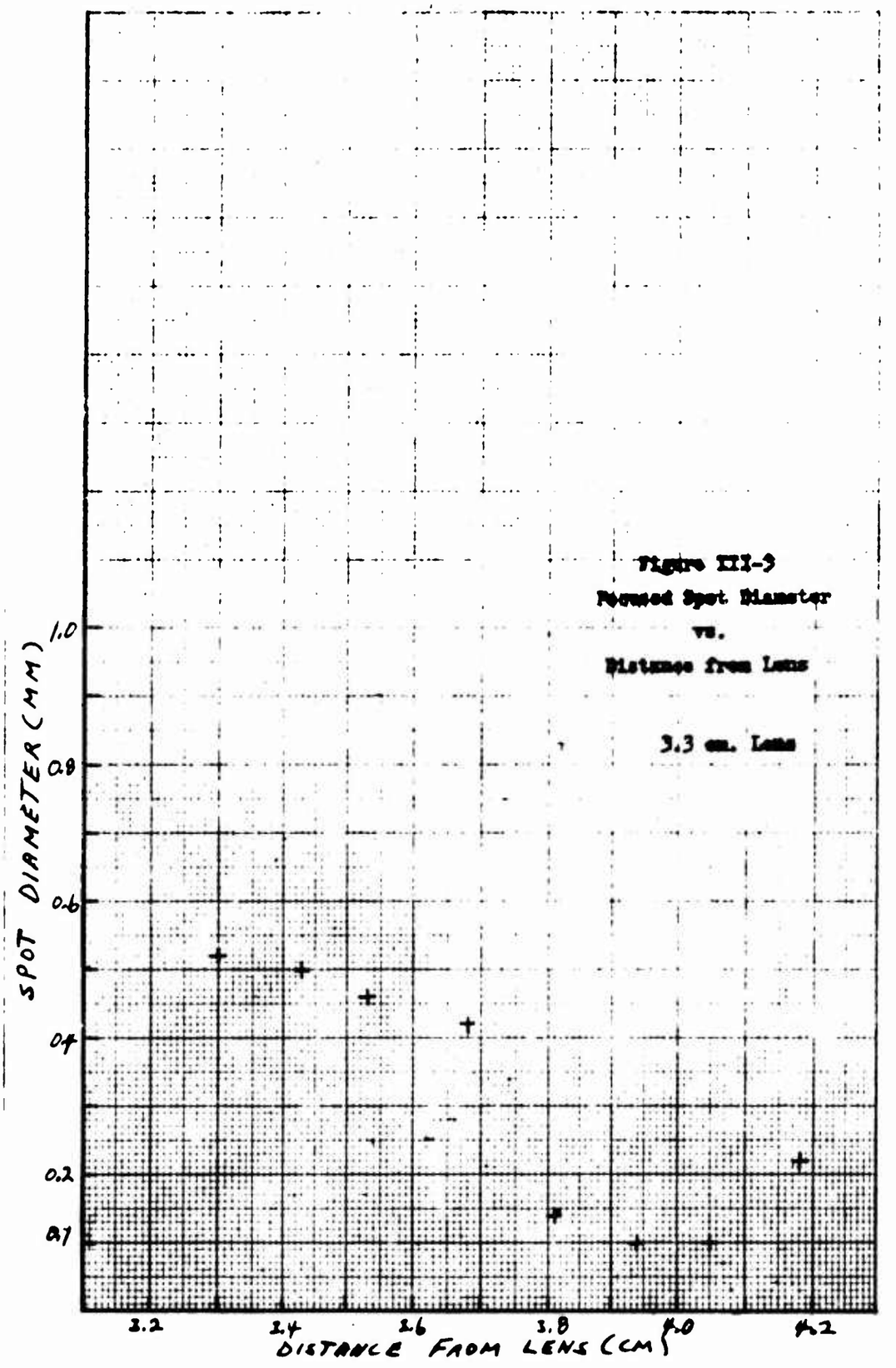
Figure III-3
Focused Spot Diameter
vs.
Distance from Lens
3.3 cm. Lens
SPOT DIAMETER (MM)
1.0
0.8
0.6
0.4
0.2
0.1
3.2
3.4
3.6
3.8
4.0
4.2
DISTANCE FROM LENS (CM)

separate the spectral wavelengths of the emission with the set-up shown in Figure III-4. Careful examination of the rate of emission during the laser irradiation would give an indication of the mechanism by which the ionization grows provided that a sufficiently sensitive photomultiplier was available. An analysis of the emission from argon ionization region revealed that the light emitted during the laser irradiation was identical to that shown in Figure III-5, and was independent of the wavelength within the visible spectrum. Both the risetime and the amplitude of the emission were dependent on the amount of energy into the gas. The risetime of the observing system was limited to about 6 nanoseconds by the Tektronix 585 oscilloscope used to record the photomultiplier signal. Measured risetimes for the initial light emission were as fast as 20 nanoseconds for high energy shots when the 12.7 cm lens was used to produce breakdown. This risetime increased to 80 nanoseconds or more as the input energy dropped to near threshold. When shorter focal length lenses (the 5.08 cm and 3.3 cm) were used to produce ionization, somewhat longer risetimes were noted. In all of this work the pressure of the argon gas was 700 torr. At this pressure no signs of a line spectrum were noticed. This is consistent with the results expected on the basis of line broadening. Essentially the Ar spectrum is so dense that line broadening of the type expected from the absorption observed would produce a continuum. The same measurements made in He (to be discussed below) showed line broadening of about 100 Å during the time of laser irradiation of the gas. This same line broadening was not present after the laser irradiation turned off.

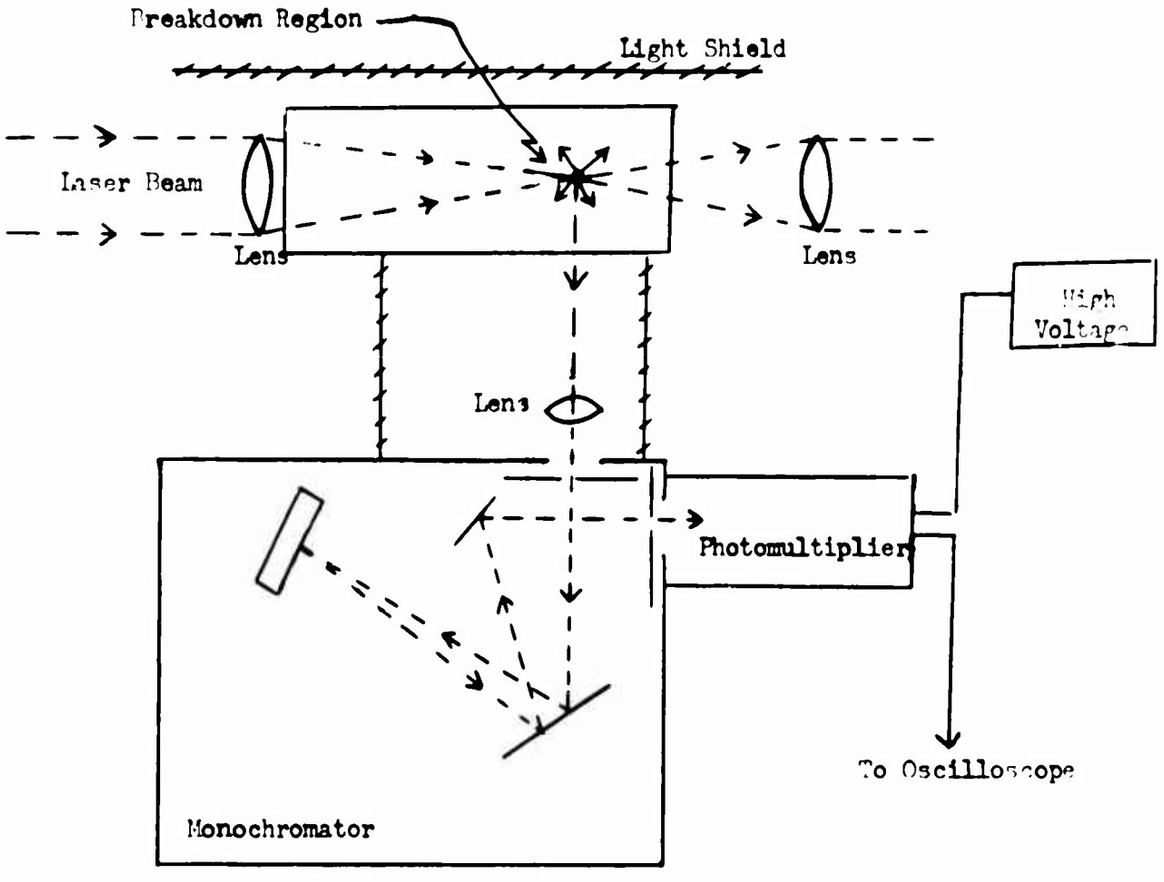

Figure III-4 Set-up to Measure Spectral Emission Wavelengths

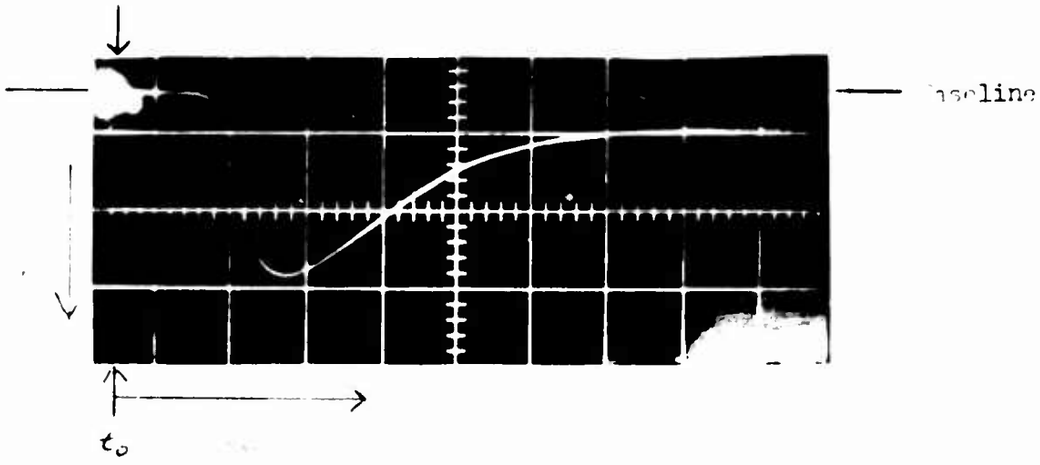

Figure III-5 Breakdown Emission from Argon While Being Irradiated with the Laser Beam (100 ns/cm horizontal; 5v/cm vertical, 4200Å)

Additional investigations were made of the time history of emission from the ionized volume after the laser radiation subsided. This emission had a time history very dependent upon the wavelength being monitored. The emission time varied from about 15 microseconds for wavelengths around 3800Å to over 200 microseconds for wavelengths around 4600Å to 5600Å and then dropping off to about 20 microseconds around 6300Å. A typical time resolved photograph of the emitted light is shown in Figure III-6.

D. IONIZATION TIME AS A FUNCTION OF FOCAL SPOT DIAMETER

To obtain an indication of the effects of the focal spot diameter a series of measurements were made using the cell filled with 700 torr of argon. Each of the lenses whose focused spot diameter had been measured previously were used to produce ionization. The curve shown in Figure III-7 illustrates the effect of spot diameter on the breakdown (attenuation) time versus peak electric field strength. Repeated experiments have shown conclusively that the threshold E_p for the 3.3 cm lens is, indeed, higher than the thresholds seen for the 12.7 cm and 5.08 cm lenses. It may be that the higher threshold is caused by an increase in the diffusion losses which accompnay the smaller focal diameter. This is supported by the fact that the average data for the 5.08 cm lens lies above the data for the 12.7 cm lens.

It should be explained that in the course of experimentation, it became necessary to increase the triggering sensitivity. This caused the addition of a small, constant increment in breakdown time measurements. In order to avoid confusion all of the data presented has been adjusted to produce the pulse peak at 125 nanoseconds from the start of the pulse. By doing this all data presented in earlier reports can be accurately compared.

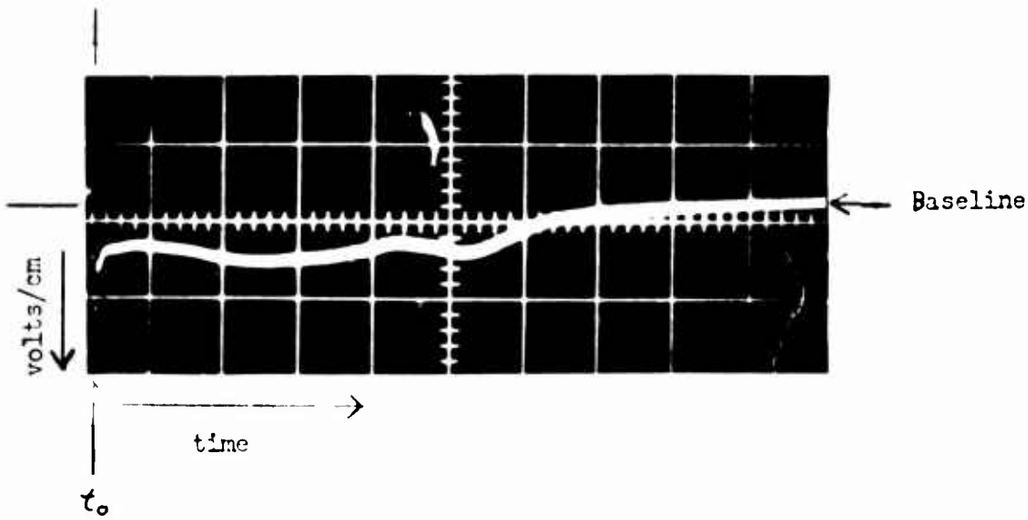

Figure III-6 Breakdown Emission from the Plasma Formed in Argon (20 u s/cm horizontal; ?v/cm vertical, 4500°)

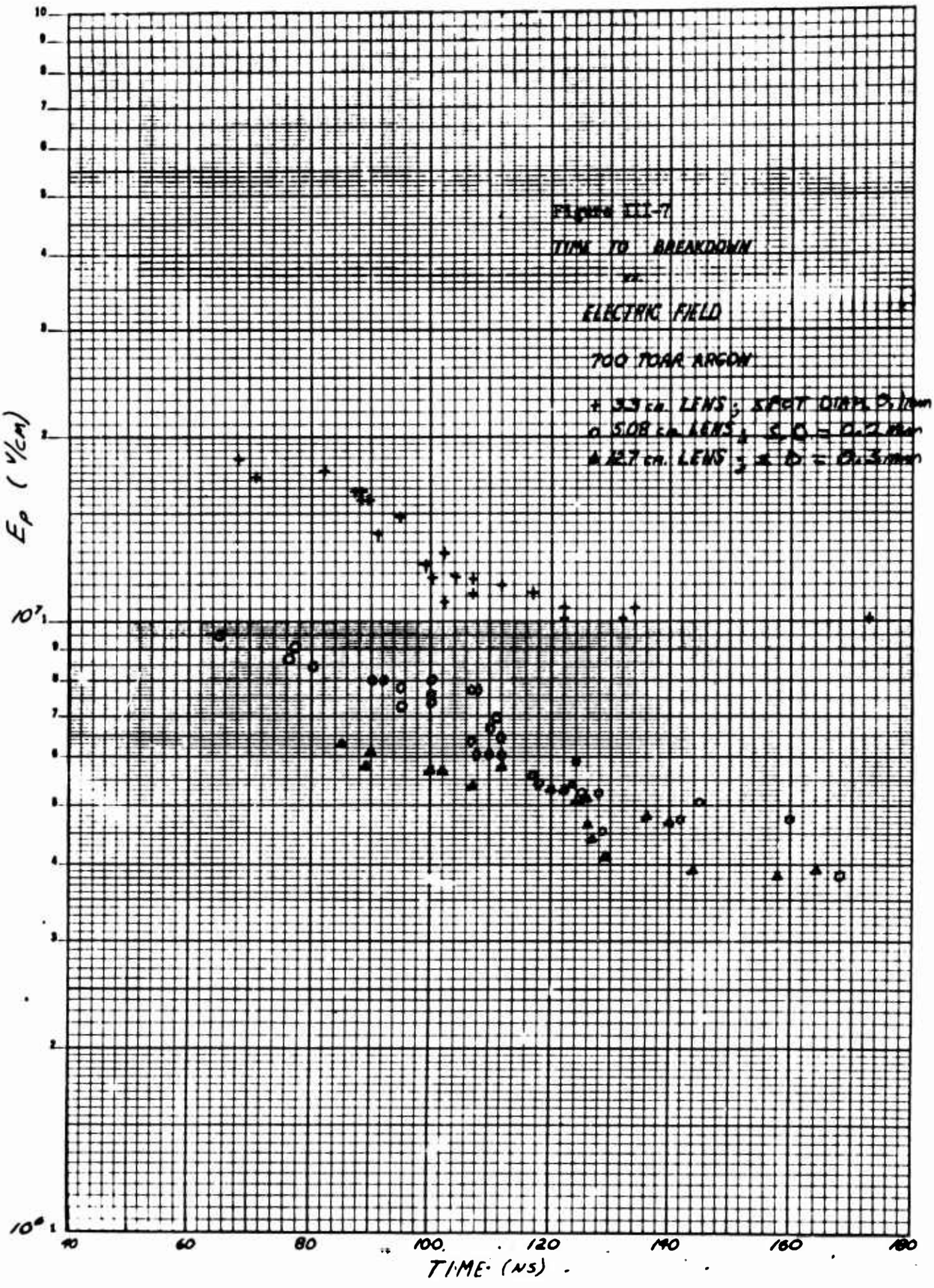
FIGURE III-7
TIME TO BREAKDOWN
vs.
ELECTRIC FIELD
700 TORR ARGON
* 3.9 cm. LENS ; SPOT DIAM. D ≤ 1.0mm
o 5.08 cm. LENS ; D ≤ 0.2 mm
Δ 12.7 cm. LENS ; D ≤ 0.3 mm
E_p (V/cm)
10^7
10^6
10
60
80
100
120
140
160
180
TIME (NS)

Peak electric field strength used for Figure III-7 has been calculated using $E_p = \sqrt{2 \frac{P}{A} Z_o}$ (Eq. III-1)

where

E_p = peak electric field

P = input power determined by dividing the half-power pulse width into the total energy

Zo = the impedance of free space

and A = the area of the half intensity contour computed using $A = \frac{\pi d^2}{4}$ where d is the half-intensity (3db) diameter measured for each lens.

B. MEASUREMENTS OF BREAKDOWN IN HELIUM

A glass cell similar to those used for argon was constructed and filled with 700 torr of helium. Attached to one side of this vessel was a small enclosed capsule of mercury sealed so that it could be opened at the desired time by a small ferrous breaker. Initially the mercury capsule remained sealed and measurements of breakdown in helium were made. The most obvious difference between argon and helium was that helium showed little or no sign of attenuation of the laser light although a spark was visible and emission was measured by the monochromator system. Because of this lack of attenuation no accurate measurement of variation in the time of breakdown occurence could be made. The time of the start of the initial light emission (from start of laser pulse) was measured for a large number of cases, and breakdown as measured by time of light emission, seemed to occur within a few nanoseconds of the peak of the laser pulse no matter how great the change of energy into the gas.

With available energy, breakdown could not be produced with the 12.7 cm lens. The breakdown threshold was determined by using the 5.08 cm lens and the 3.3cm lens. Knowledge of the spot size of each of these lenses enabled the field strength to be computed.

The threshold determined for helium using equation III-1 was 7×10^6 volts/cm as compared to 3.9×10^6 volts/cm for argon. The pressure in both cases was 700 torr; however, the 12.7 cm lens was used to determine the Ar threshold while the 5.08 cm lens was used to determine the He threshold.

An attempt was made to determine the effects upon breakdown caused by a large amount of mercury vapor. To do this the mercury ampule attached to the cell was broken and the mercury vapor was allowed to mix with the helium gas. At room temperature and below no effects in the helium breakdown were observed. After heating the ampule to drive mercury vapor into the cell it was possible to detect a noticeable effect on the breakdown emission. Whereas a line spectrum was observed in pure helium, a continuum became evident when mercury was added. It was observed that when the field strength was below the threshold of helium a continuum with superimposed Hg lines was predominant whereas, when the field strength was above the threshold for helium, the helium lines (notably 4685Å) were superimposed on the mercury continuum. Any tendency of the mercury impurity to lower the threshold could not be detected above the emission from the Hg. It is difficult to determine whether the initiation of breakdown takes place in the main gas (He) or in the impurities present in the main gas. The addition of Hg to easily observable gases such as argon may give more indication of the effects of impurities.

Photographs were taken to record the time history of the breakdown emission of pure helium during the time of irradiation from the laser. These curves (an example shown in Figure III-8) compare rather well with those from the breakdown in argon at the same pressure. A record of the entire emission from the breakdown region of the helium is shown in Figure III-9. No explanation can be offered for the shape of the emission curve at late times.

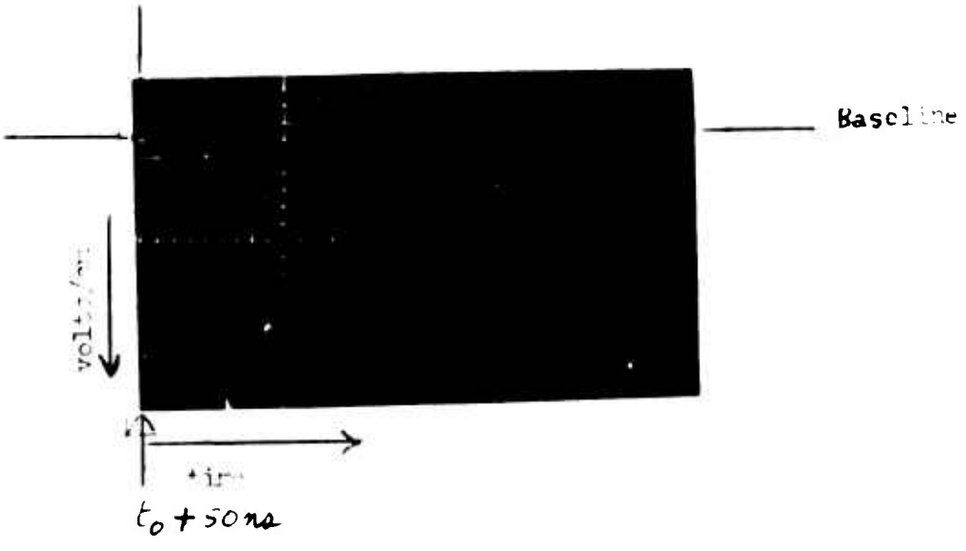

Figure III-8 Breakdown Emission From Helium During the Time of Laser Irradiation
(50ns/cm horizontal; 5V/cm vertical; 4(8854))

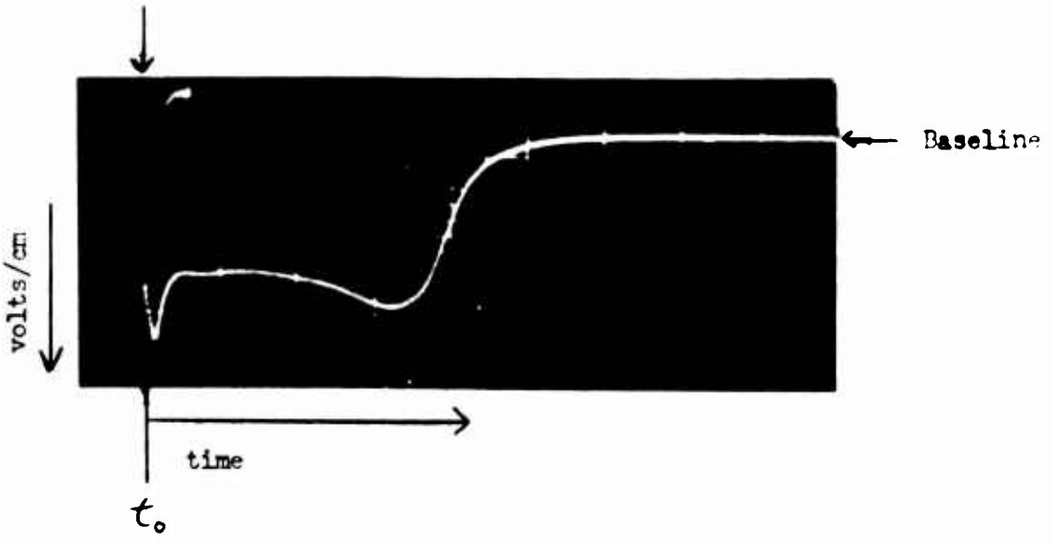

Figure III-9 Breakdown Emission from Plasma Formed in Helium
(10 us/cm horizontal; 1v/cm vertical 4685Å)

Portion of curve shown in III-8 cannot be seen in this curve because of its sharp rise, short duration, and high amplitude.

F. SOME OBSERVATIONS AT LOW PRESSURE

As pressure is lowered the diffusion loss from the breakdown region becomes greater, and at some pressure becomes great enough to prevent the avalanche buildup. If one carefully measures the number of charges produced as the pressure is varied below the avalanche region an indication of the ionization build-up process may be obtained. In order to make measurements at low pressures a glass cell was constructed and evacuated to 10^{-7} torr.

This cell (residual gas air) had a mercury ampule and the planned work was to increase the vapor pressure in the cell by increasing the temperature of the mercury ampule. Electrodes were provided to collect the charge produced.

Before the mercury was allowed into the cell several laser shots produced 10^{10} charge pairs. After several shots this level dropped two orders of magnitude and remained at 10^{8} charges throughout a series of shots. Thereafter no change was noted when the mercury was allowed to enter the cell and raised in vapor pressure to 10^{-2} torr. The charge collection current was different at all of these pressures than it was at 700 torr. The current had three peaks spaced about 10us apart and increasing in amplitude with time. It is not yet clear what causes this shape or why increasing the pressure of Hg had no effect. Perhaps reflected light from the rear of the cell produced photo electrons from the electrodes which were collected. This work indicates that low pressure investigations may produce interesting results, and may perhaps provide some answers to the initiating and growth mechaniams provided more care in experimentation is taken. Low pressure work will be continued for various other gases. Additional precautions to eliminate unwanted variables will be taken.

G. EFFECTS OF HIGH AND LOW PRESSURE

A test cell (See figure III-10) capable of withstanding pressures of 1500 psi has been constructed and is being used to investigate gas ionization as a function of pressure. Constructed of stainless steel, the cell is capable of being evacuated to 10^{-6} mm Hg before being filled with the desired gas. A Heise guage is being used to monitor the pressure accurately ($\pm$0.5 psi) from atmospheric to 1000 psi. An additional glass cell system capable of evacuation to 10^{-9} mm Hg has been constructed for the low pressure work. This cell and associated equipment are shown in Figure III-11.

H. CONCLUSIONS

The process of gas ionization shows a threshold dependence upon the intensity distribution in the laser beam. Since significant changes in the intensity distribution can cause significant changes in spot size, care must be taken to monitor these variations. Secondly, spot size for short focal length lenses cannot be determined from a knowledge of beam divergence, thus accurate measurements of spot size is an important parameter to be defined experimentally. Reducing the spot size by use of a 5.08 cm focal length lens lowered the time of breakdown for a given field strength as compared to that for a 3.3 cm lens.

Results of the work done in helium indicate that the spectral emission of the plasma differs for the various gases. The easily ionizable mercury vapor had no detectable effect on the breakdown time in helium.

I. FURTHER WORK

It is planned to investigate the entire pressure range agreed upon using several pure gases (Argon, Nitrogen, Helium and air). Work is also anticipated to determine the effects of a neodymium frequency (1.06u) pulse on several gases.

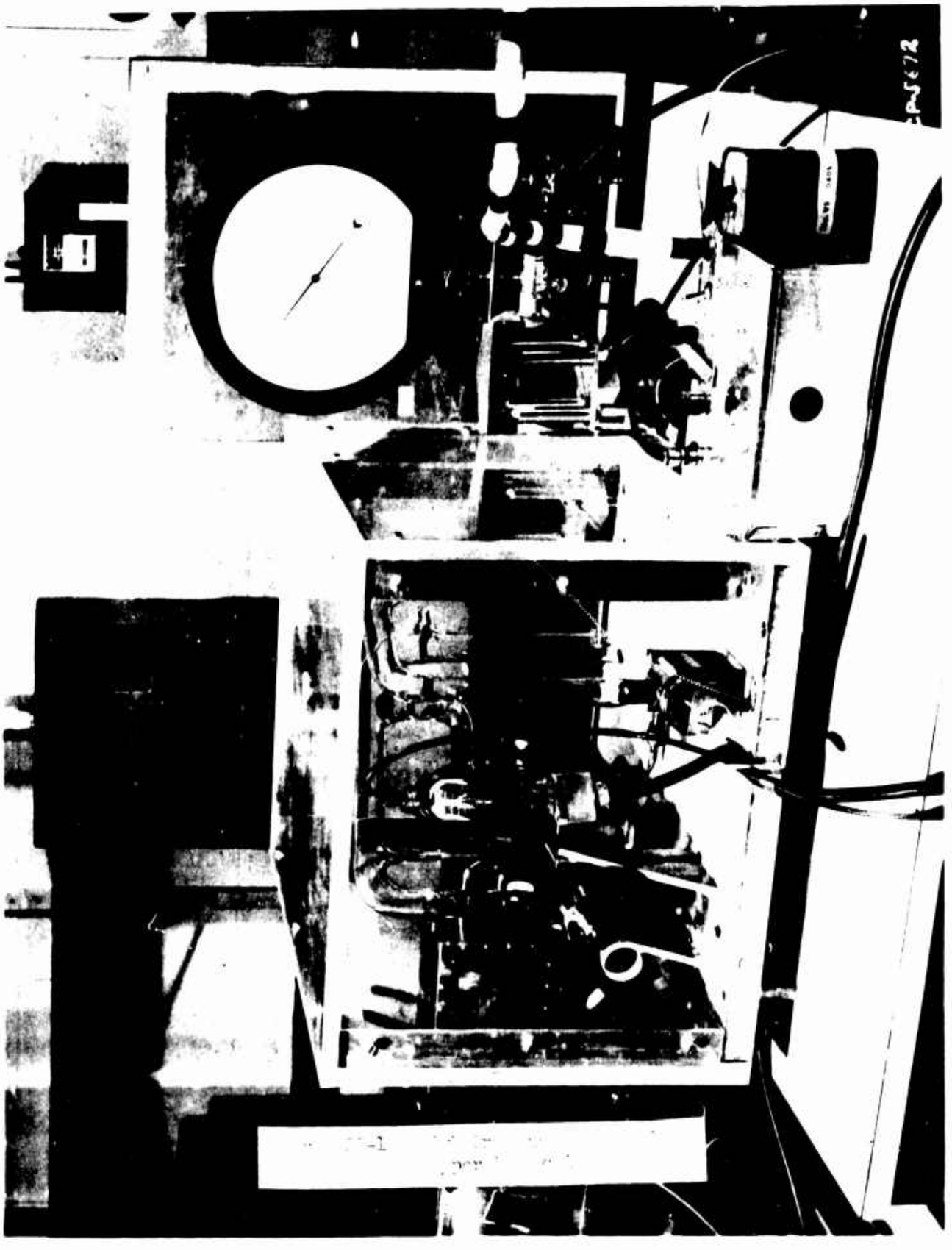

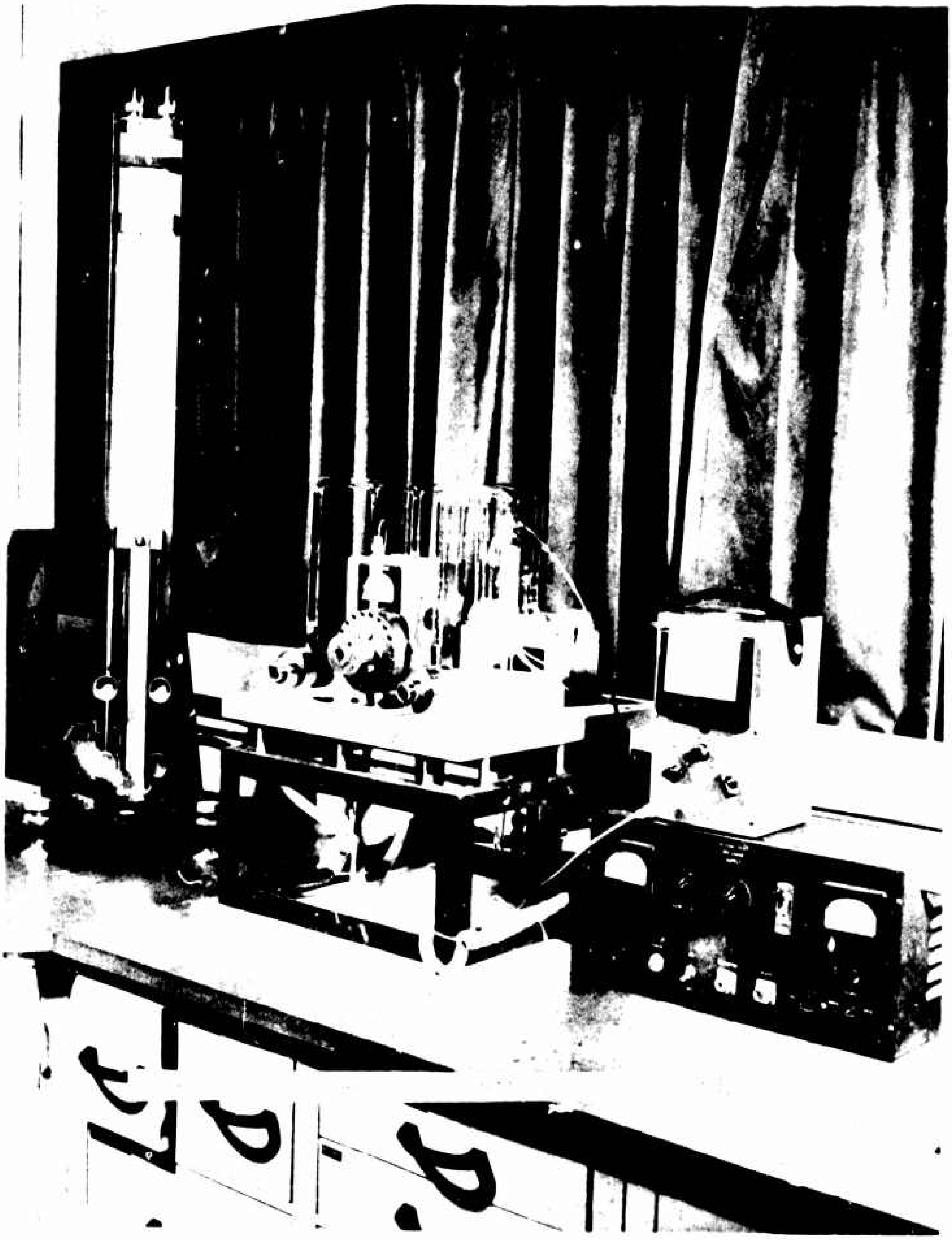

IV. THEORETICAL INVESTIGATIONS *

A. INTRODUCTION

In previous discussions [1,2] of the breakdown of gases by lasers we have considered various aspects of the hypothesis that at high gas pressures ($\sim$ one half atmosphere and above) the breakdown is the result of initiation by a multi-photon ionization event followed by an avalanche type growth of the ionization to the observed value. In this section we will consider further the avalanche type growth of the ionization. We will assume that for the gases under consideration an electronically excited atom is rapidly ionized by multi-photon absorption so that the effective rate of ionization is equal to the rates of electronic excitation plus ionization by electron impact. This assumption needs to be investigated further but appears to be reasonable.

The topics to be considered in this section are:

B. Further evidence concerning the applicability of the extension of microwave theory to the laser breakdown problem as obtained from steady state and time dependent treatments of the photon absorption process using simplified models for the electron-gas atom collisions,

C. The calculation of avalanche growth constants for Ar and N_2 using the extended microwave theory, and

D. The calculation of approximate curves of the threshold laser intensity required for breakdown as a function of gas density, laser pulse length and focal spot size.

---

* This discussion is by A. V. Phelps.

B. Equivalence of Discrete Photon and Microwave Theories

Published discussions [3] of laser induced breakdown differ considerably as to the applicability of extensions of microwave theory to optical frequencies for the calculation of the rate of growth of the ionization. We have shown previously [1] that the differential formulation of the Boltzmann equation used in the microwave calculations is a good approximation to the difference form of the Boltzmann equation appropriate to the absorption of photons in free-free transitions, provided that the electron energies of importance are large compared to the photon energy, and that the electron energy distribution function does not change too rapidly in an energy interval equal to the photon energy. In practice, this means that we expect the microwave theory to give good values for the rates of excitation but possibly to yield ionization rates which are too low. As further evidence for the correctness of this prediction we shall compare directly solutions of the difference and differential forms of the Boltzmann equation using approximate forms for the cross section for photon absorption and electron excitation. Using one such model we shall inquire as to what a steady state solution tells us about the rate of excitation due to the absorption of a finite number of photons as compared to the rate calculated using the microwave theory. This investigation is largely in response to the suggestion [4] that because the ionization or excitation potential is a relatively small multiple of the photon energy, the electrons may gain sufficient energy to excite or ionize without suffering the randomizing effects of large numbers of collisions implied by the differential form of the Boltzmann equation. This analysis has been carried out using

random walk theory by Drs. . P. Gaver and J. A. Marshal of the Laboratories Mathematics Department.[5] The second model allows a solution of the time dependent difference equation.

(A) Steady State Solution

The Boltzmann equation on which the statistical analysis is based is Eq. (6) of Ref. 1. If we assume that the electron energy distribution function consists of a series of delta functions[6] separated by the photon energy $h\nu$, then Eq. (6) of Ref. 1 becomes

$$\left.\frac{dP_i}{dt}\right|_{photon} = \mu_{i+1}P_{i+1} - \mu_i P_i + \lambda_{i-1}P_{i-1} - \lambda_i P_i \quad , \quad (1)$$

where the index i is an integer, P_i is the fraction of the electrons with an energy of $\varepsilon_i = ih\nu$, λ_i and μ_i are the probabilities for the absorption and stimulated emission of a photon by an electron with an energy $\varepsilon_i = ih\nu$. From Eq. (5a) of Ref. 1 an approximation to λ_i valid for $h\nu << \varepsilon_i$ and low ε_i is

$$\lambda_i = \frac{2}{3}\frac{\varepsilon_o}{h\nu}\frac{\varepsilon_i}{h\nu}\nu_m(\varepsilon_i) \quad , \quad (2)$$

where $\varepsilon_o = e^2E^2(mw^2)^{-1}$ is the classical oscillatory energy of a free electron and $\nu_m(\varepsilon_i)$ is the frequency of momentum transfer scattering collisions of electrons by the gas molecules. At present we do not have accurate expressions for λ_i and so will consider a second approximation to λ_i which is probably better when $h\nu$ and ε_i are comparable. This relation has been suggested by Holstein[7] and is

$$\lambda_i = \frac{2}{3}\frac{\varepsilon_0}{h\nu}\frac{(\varepsilon_i + \frac{h\nu}{2})}{h\nu}\nu_m\left(\varepsilon_i + \frac{h\nu}{2}\right) . \quad (3)$$

In order for the electron distribution to be limited to the discrete set of P_i's the energy loss in excitation ε_x is assumed to be equal to an integral multiple of $h\nu$, i.e., $\varepsilon_x/h\nu = H$. From the detailed balancing argument given in Eq. (7) of Ref. 1, we have

$$(i-1)^{1/2}\lambda_{i-1} = i^{1/2}\mu_i . \quad (4)$$

In order to simplify the problem we will assume that excitation occurs as soon as the electron reaches the level H. This is equivalent to the assumption of an infinite excitation cross section discussed by Allis.[8] In the microwave case this approximation has been found to give reasonably accurate excitation rates at electric field intensities which are not too high[3].

The frequency of exciting collisions using the model described above is equal to the reciprocal of the expectation value of the first passage time[5]. This quantity, E(T|H), is given by [5]

$$E(T|H) = \sum_{i=0}^{H-1}\sum_{j=0}^{i}\frac{\left[j^{1/2} + (j+1)^{1/2} + \cdots + 2^{1/2} + 1^{1/2}\right]}{j^{1/2}\lambda_j} \quad (5)$$

Equation (5) has been evaluated as a function of H for various assumed dependence of λ_i. In this discussion we will consider three cases;[9]

$$\text{a)}\quad \lambda_i = \frac{2}{3}\frac{\varepsilon_o}{h\nu}\frac{(\varepsilon_i + \frac{h\nu}{2})}{h\nu}\nu_a = (i+\tfrac{1}{2})\lambda_a \qquad (6a)$$

$$\text{b)}\quad \lambda_i = \frac{2}{3}\frac{\varepsilon_o}{h\nu}\frac{(\varepsilon_i + \frac{h\nu}{2})}{h\nu}\left(\frac{h\nu}{\varepsilon_i + \frac{h\nu}{2}}\right)^{3/2}\nu_b = \frac{\lambda_b}{(i+\frac{1}{2})^{1/2}} \qquad (6b)$$

$$\text{c)}\quad \lambda_i = \frac{2}{3}\frac{\varepsilon_o}{h\nu}\left(\frac{\varepsilon_i}{h\nu}\right)\left(\frac{h\nu}{\varepsilon_i}\right)^{3/2}\nu_c = \frac{\lambda_c}{i^{1/2}} \qquad (6c)$$

Case a) corresponds to the substitution in Eq. (3) of an energy independent frequency of momentum transfer collisions such as found for electron-neutral collisions in H_2 and H_e at energies above a few electron volts. This is expected to be the most realistic of the models considered here since electron-neutral collisions dominate the photon absorption process during the growth of ionization. We note that the use of the constant collision frequency assumption in Eq. (2) for our simple model leads to $\lambda_o = 0$ and trapping of electrons at zero energy and so is unrealistic. Cases b) and c) correspond to the assumption of electron scattering by ions in which the collision frequency is approximately inversely proportional to the 3/2 power of the electron energy.[10] Case (c) is of interest because it leads to $\lambda_o = \infty$ and because it is a case which one would expect to find treated by others.[4,11] In addition for case (c) $\lambda_i = \mu_i$ in Eq. (1) so that the electron motion in energy is a pure random walk. Rather than show the calculated excitation rates directly, we will compare them with the results of the differential or microwave theory.

The solution to the differential form of the Boltzmann equation for the simple model considered here is obtained by setting the right hand side of Eq. (9) of Ref. 1 to zero, solving for $f(\varepsilon)$ and then normalizing.

It can be shown that this procedure leads to the relation

$$\frac{1}{\nu_x} = \frac{2}{3(h\nu)^2} \int_0^{\varepsilon_x} \frac{\varepsilon \, d\varepsilon}{\lambda(\varepsilon)} \tag{7}$$

For case (a), $\lambda(\varepsilon) = \lambda_a \left(\frac{1}{2} + \frac{\varepsilon}{h\nu} \right)$ (8a)

and $$\frac{\lambda_a}{\nu_x} = \frac{1}{3} \left[\frac{2\varepsilon_x}{h\nu} - \ln \left| \frac{2\varepsilon_x}{h\nu} + 1 \right| \right] \tag{9a}$$

For case b), $\lambda(\varepsilon) = \lambda_b \left(\frac{1}{2} + \frac{\varepsilon}{h\nu} \right)^{-1/2}$ (8b)

and $$\frac{\lambda_b}{\nu_x} = \frac{4}{45} \left[\left(\frac{3\varepsilon_x}{h\nu} - 1 \right) \left(\frac{\varepsilon_x}{h\nu} + \frac{1}{2} \right)^{3/2} + \left(\frac{1}{2} \right)^{3/2} \right] \tag{9b}$$

For case (c) $\lambda(\varepsilon) = \lambda_c \left(h\nu / \varepsilon \right)^{1/2}$ (8c)

and $$\frac{\lambda_c}{\nu_x} = \frac{4}{15} \left(\frac{\varepsilon_x}{h\nu} \right)^{5/2} \tag{9c}$$

The ratio of the excitation frequency calculated using Eq. (5) to that given by Eqs. (9a, b, c) is shown in Figure IV-1. The lower curve shows that for the model of electron-neutral scattering in which the electron collision frequency is independent of energy, [12] the excitation frequency using the discrete model is lower than that calculated for the continuous model by roughly 30%. In the model of electron-ion scattering the dashed curves show that the calculated excitation frequency for the discrete case is generally, but not always, higher than that calculated

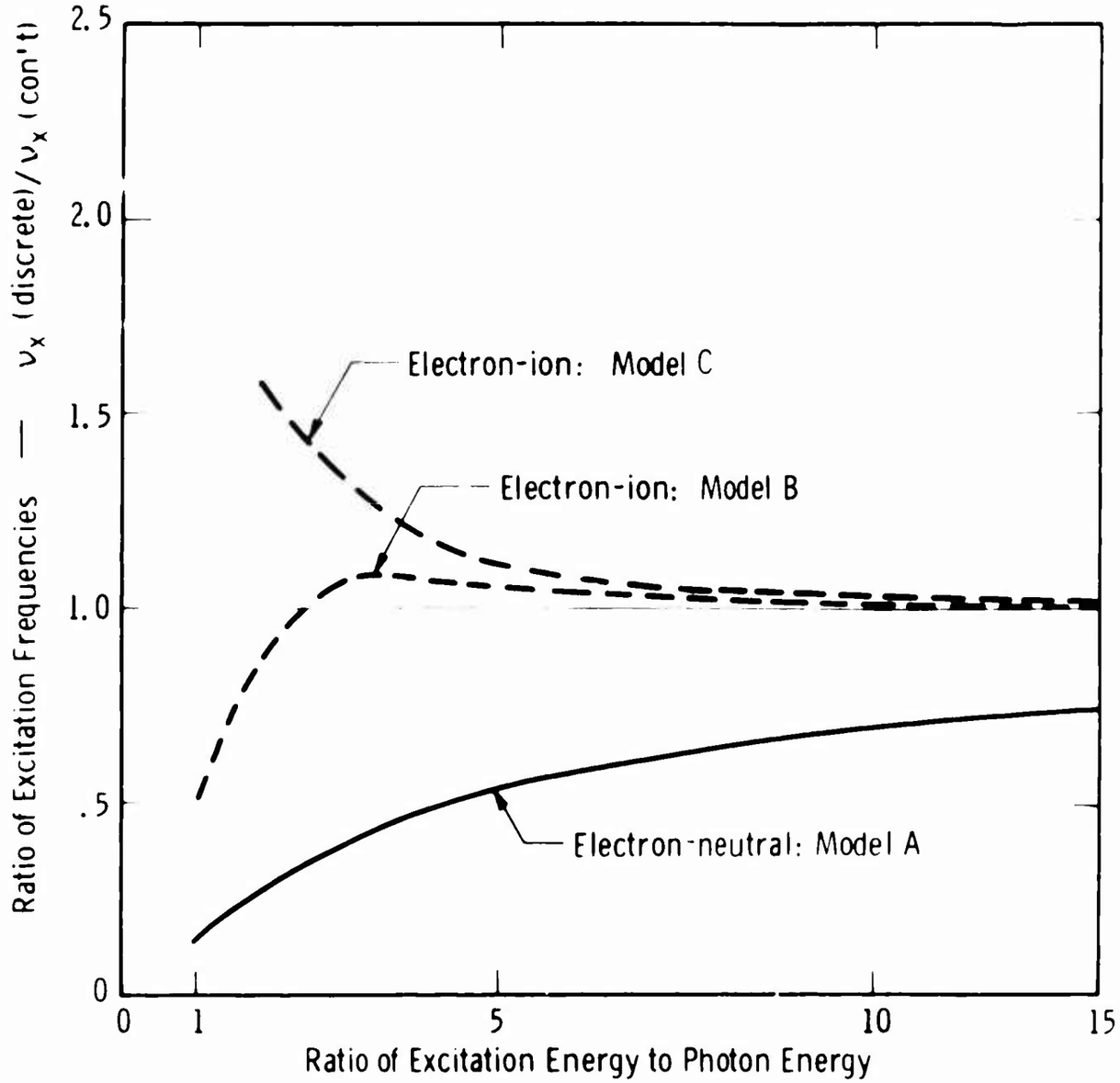

FIGURE IV-1 Ratio of Excitation Frequencies Calculated by Continuous Theory and by Discrete Photon Absorption Theories

by the continuous case. For $\mathcal{E}_x/h\nu \geq 5$ the difference is less than 1%. Since these calculations show that the error resulting from the use of the continuous theory depends strongly on the energy dependence of the absorption probability, it is very desirable to carry out calculations of the rates of excitation using more realistic cross sections using the difference form of the Boltzmann equation. Such a calculation is being attempted but so far has been unsuccessful.

(b) Time Dependent Solutions

As an additional check on the applicability of the extended microwave theory to the prediction of the rate of growth of ionization due to the absorption of photons, we have calculated some time dependent electron energy distribution functions and excitation frequencies. These values can then be compared with the results of the usual microwave theory which assumes that electron energy distribution is independent of time. The model used in these calculations is more exact than that discussed above in that the probability of an excitation collision is finite, although of simple analytical form.[13] As above, we neglect the energy loss in elastic collisions with the gas atoms, although this loss is expected to be important at high pressure in the rare gases.[14] The equations which have been solved are:

$$\frac{dP_i}{dt} = \mu_{i+1} P_{i+1} - (\mu_i + \lambda_i) P_i + \lambda_{i-1} P_{i-1} - B_i P_i + \sum_{j=M}^{M} B_j P_j \delta(i-1) , \tag{10}$$

where $B_i = (i - H)\,P$ for $i \geq H$; $B_i = 0$ for $i < H$; $\lambda_i = i\lambda$ for $i \neq M$; $\lambda_M = 0$; $\delta(i-1) = 1$ for $i = 1$; $\delta(i-1) = 0$ for $\delta \neq 1$ and $(i-1)^{1/2}\lambda_{i-1} = i^{1/2}\mu_i$. Note that here we have used the form of the constant collision frequency approximation corresponding to Eq. (2). This simpler approximation [9] is possible since with the present model inelastic collisions and stimulated photon emission do not populate the level at $\varepsilon_i = 0$. We note that the system of equations is terminated at $i = M$, where M is chosen by trial and error to be large enough so that the populations at energies of interest are independent of M. We can use the calculated P_i values to determine the excitation frequency using the relation

$$\gamma_x = \sum_{j=H}^{M} B_j P_j \tag{11}$$

Finally [15] we note that our assumption as to the energy dependence of B_i is equivalent to assuming that the cross section for excitation, Q_x, is given by

$$N v Q_x = \frac{(\varepsilon - \varepsilon_x)}{h\gamma} B\lambda \tag{12}$$

where $v = 5.93 \times 10^7 (\varepsilon)^{1/2}$ cm/sec. For He and electron energies within a few electron volts of the excitation threshold $\varepsilon_x/h\gamma = H = 11$, and $B\lambda \approx 1.4 \times 10^{-9} N$ sec^{-1}. The calculations given below have been carried out by D. P. Wei of the Laboratories Computer Group.

The results of the solution of Eqs. (10) are shown in Figure IV-2 where P_i is plotted as a function of $i = \varepsilon_i/h\gamma$ for B = 15. These

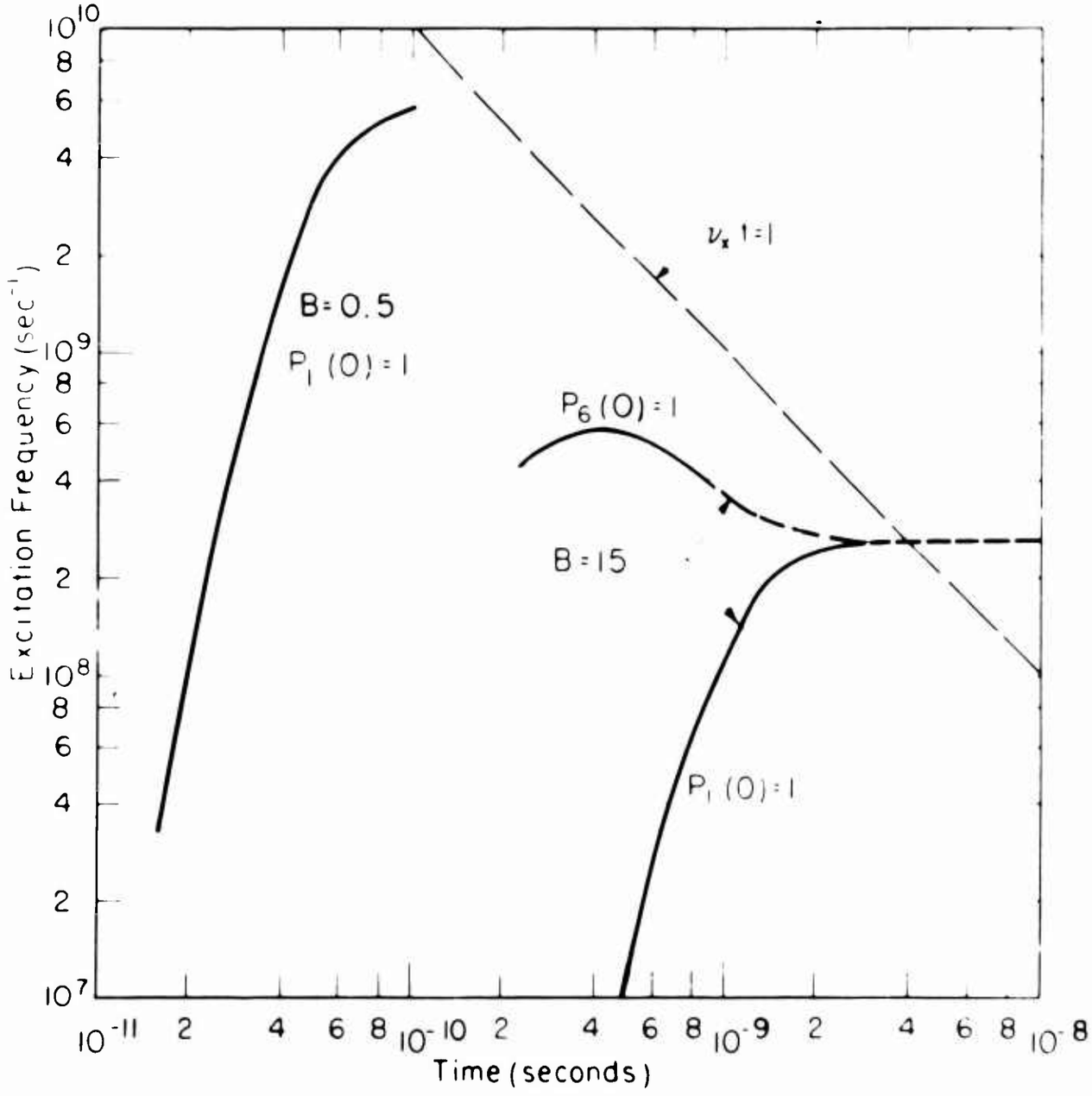

Figure IV - 2 Excitation Frequency vs. Time for Various Models

results are for the case in which $P_1 = 1$ at $t = 0$. Here time t is measured in units of $1/\lambda$ such that $T = \lambda t$. We see that the distribution function has reached its steady value by $T = 6$. Using Eq. (2) and $\gamma_i = 7.2 \times 10^{-9} N$ cm^3/sec as expected for helium at a gas density N, the curves in Figure IV-2 correspond to the case of a field strength $E = 3.8 \times 10^6$ v/cm at the laser frequency corresponding to 6943 Å or a laser power of 3.2×10^{10} watt/cm^2 and to a gas density of 2.45×10^{19} atoms/cc or one atmosphere at 300°K. In this case $\lambda = 2.3 \times 10^9$ sec^{-1} so that the distribution function has reached its final form by about 2.5×10^{-9} sec.

In the present problem we are primarily concerned with the time dependence of the excitation frequency as shown in Figure IV-3. The lower two curves (B = 15) show the γ_x values calculated using Eq. (11) for the model discussed above for helium and for two different assumptions as to the initial state of the electron, i.e., $P_6 = 1$ at $t = 0$ and $P_1 = 1$ at $t = 0$. We see that the excitation frequency has reached its final value of 2.6×10^{-8} sec by about 2.5 nsec. The upper curve shows the excitation frequency calculated for B = 0.5 corresponding to helium at atmospheric pressure and to a laser field strength of 2×10^7 v/cm or 1.06×10^{12} watt/cm^2. This calculation has not been carried to completion because of the large amount of computer time required but it appears that the excitation rate at 10^{-10} sec is significantly below the final value. The time required to attain the steady state excitation rate is important because each new electron in the avalanche will have to undergo such a transient period. The average excitation rate is therefore an appropriate integral over the instantaneous excitation rate weighted according to the probability of finding a new electron in a given initial state after the photoionization of the excited atom.[16] We have not carried out this

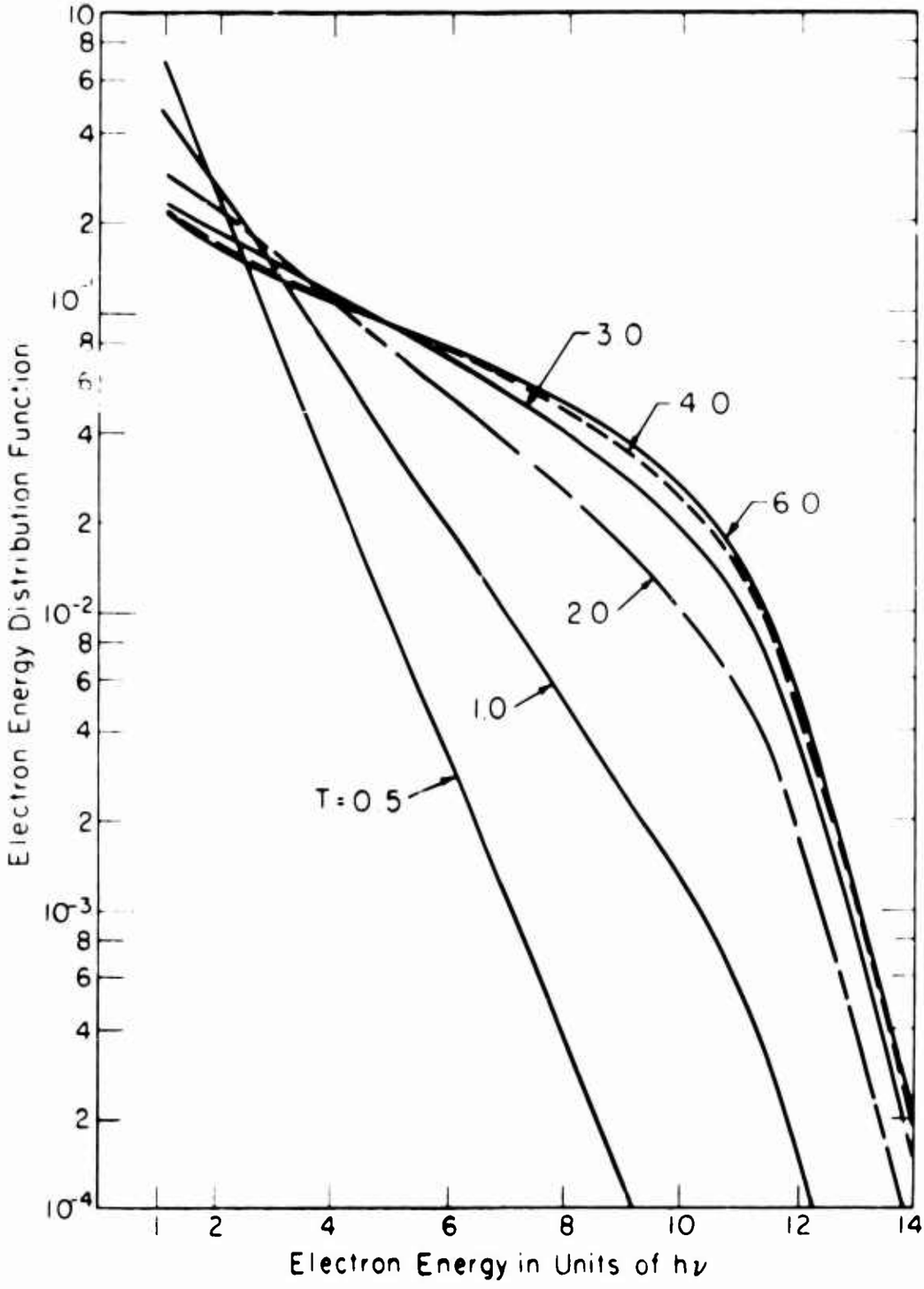

Figure IV - 3 Time Dependent Electron Energy Distributions

calculation. This average excitation frequency will generally be smaller than the final value because this calculation is one way of allowing for the energy required to raise the energy of each new electron to the mean electron energy.[16]

We now wish to compare the final excitation rates with those calculated using other approximate models. Using the steady state solution corresponding to the time dependent calculations, i.e. Eq. (2) with ν_m independent of energy and the summations in Eq. (5) going from 1 to H, we find ν_x/λ = 1.1[illegible] x 10^{-1} compared to a final value of 1.2 ± 0.5 x 10^{-1} using the time dependent solution for E = 15. The agreement between these results is expected since they are based on models which are negligibly different. The constant collision frequency model using Eq. (3) in Eq. (5) yields ν_x/λ = 1.1[illegible] x 10^{-1} due to the slightly smaller values of λ_i/λ over the range of i considered (0 to H rather that 1 to H + 1). The solution to the differential form of the Boltzmann equation gives ν_x/λ = 1.57 x 10^{-1} and 1.59 x 10^{-2} when Eqs. (2) and (3), respectively, are substituted into Eq. (2) and ν_m is constant. The extended microwave theory using realistic cross sections as discussed in Ref. 1 gives ν_x = 1.5 x 10^{8} sec^{-1} or ν_x/λ = 6.6 x 10^{-2}. This lower value is largely the result of the neglect of energy loses due to elastic collisions in the simple models we have considered in this section. Finally, we note that the steady state value of ν_x/λ for B = 0.5 is greater than 9 x 10^{-2} as compared to the microwave values of ν_x = 6.1 x 10^{9} sec^{-1} or ν_x/λ = 9.7 x 10^{-2}. In this case elastic collisions are much less important than in the lower electric field (higher E) case. These calculations again suggest the possibility of significant differences between steady state

excitation rates using the two forms of the Boltzmann equation. However, they show that a really valid comparison can be made only when better models are used to account for the effects such as elastic collisions and the energy required to heat up the new electrons.

C. Avalanche Growth in Ar and N_2

In this section we present the results of calculations of coefficients governing the rate of growth of ionization in Ar and N_2 and in the case of Ar we apply these results to the prediction of the time required for breakdown in Ar under simplified experimental conditions. The notation and simplifications here are identical with that of Ref. 1 and will not be repeated here.

Figure IV-4 shows values of the excitation and ionization frequencies per atom and the electron diffusion coefficient at unit density for Ar at frequencies such that $\omega >> \nu_m$. These calculations were made using the cross sections and computer program discussed by Engelhardt and Phelps.[17] Figure IV-5 shows the calculated excitation, ionization, and diffusion frequencies for electrons in Ar at one atmosphere pressure at 300°K as a function of the field strength of the ac field at the frequency of a ruby laser (6943 Å). These curves are then used to calculate the curves shown in Figure IV-6 of the time required for the ionization to grow by an avalanche process from 1 electron in the focal volume ($\sim 10^5$ electron/cc) to complete ionization. As discussed in Ref. 1 the solid curves are calculated under the assumption of electron loss by free diffusion to the cylindrical boundary of the focal volume while the dashed curves correspond to negligible diffusion loss as when ambipolar diffusion is important.

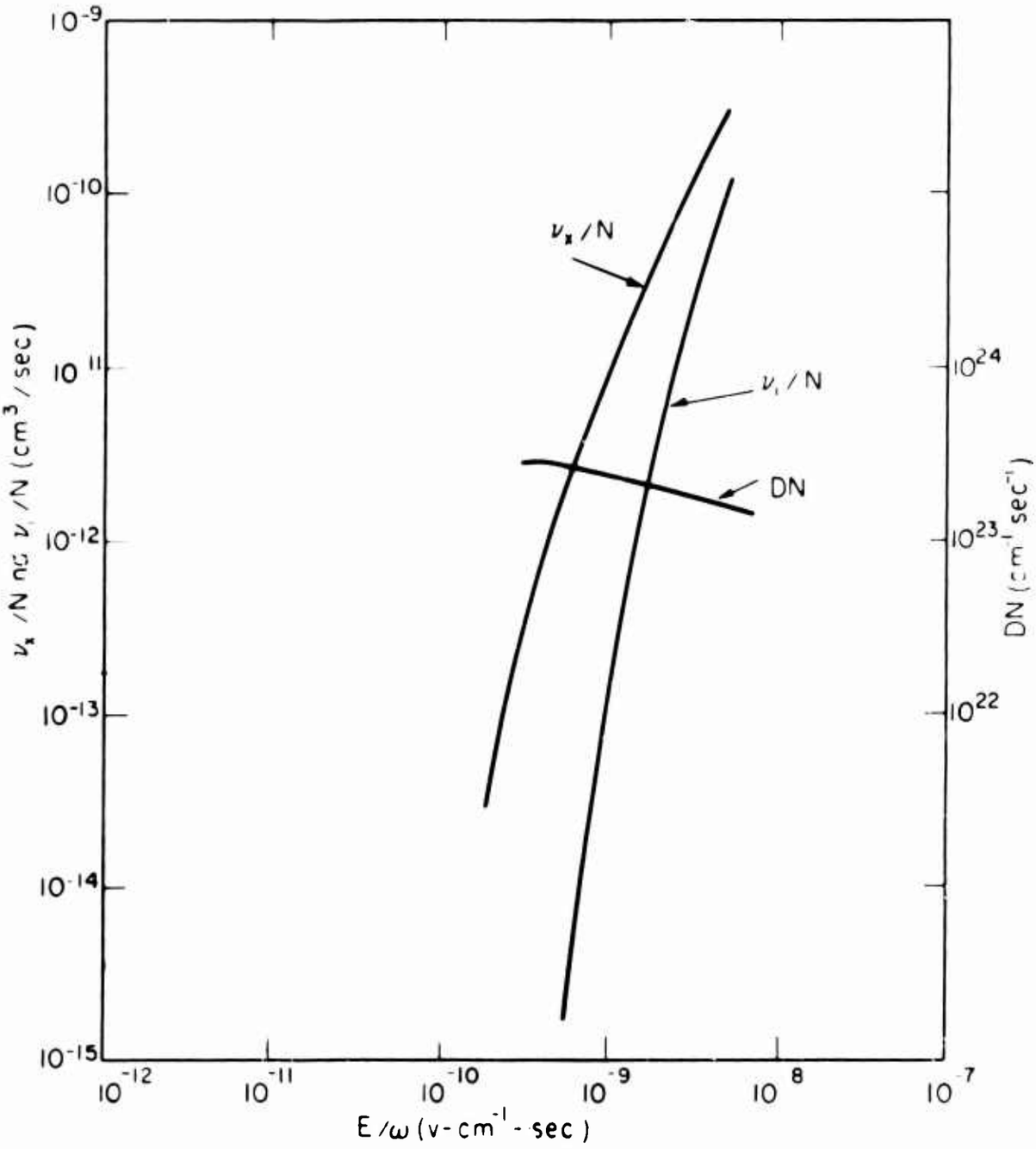

Figure IV - 4 **Very High Frequency Excitation, Ionization and Diffusion Coefficients for Argon**

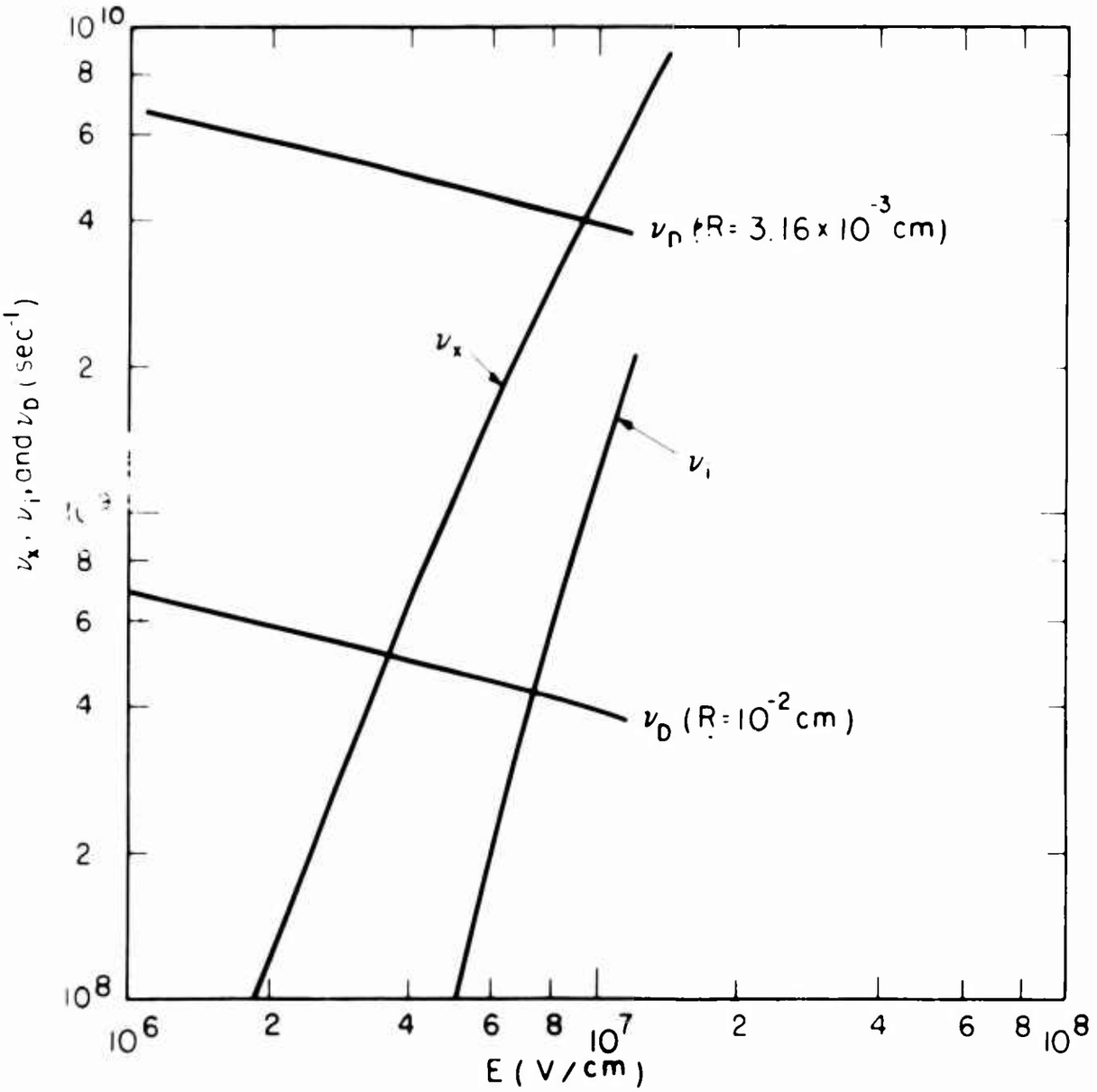

Figure IV - 5 Excitation, Ionization and Diffusion Frequencies for Argon at One Atmosphere, 300°K at 6943 Å Using Microwave Theory

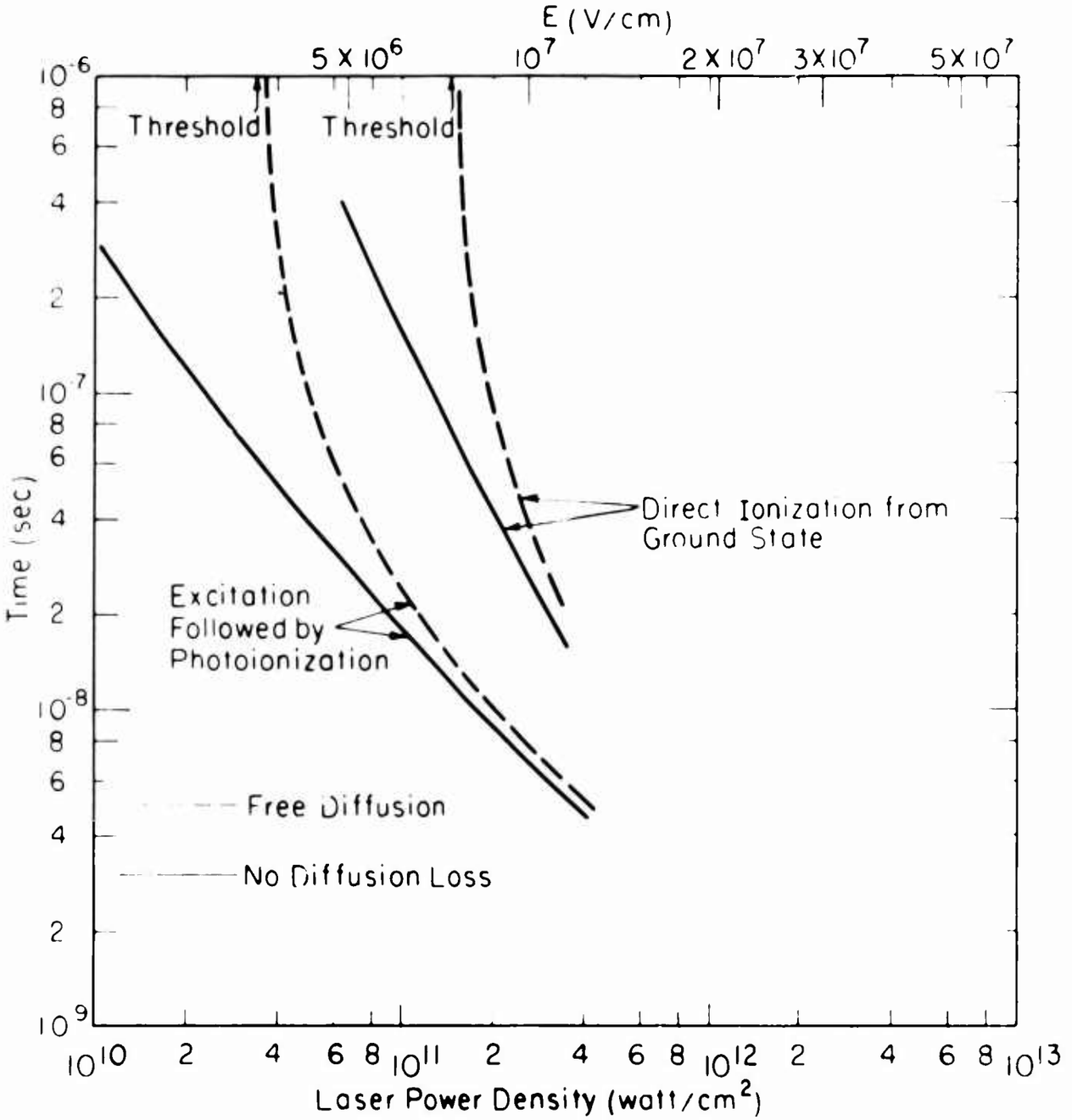

Figure IV - 6 Time Required for Laser Breakdown in Argon at One Atmosphere and 10^{-2} cm Radius Focal Volu

It is still rather risky to compare the results of this theory with experiment because of the uncertainties in the time of initiation of the avalanche, the spatial and time variations in the laser power density which are not included in the theory, and the uncertainties remaining in the applicability of the extended microwave theory. However, we note that the threshold field strength shown in Figure IV-6 for free electron diffusion and excitation followed by photoionization, i.e. 3.2×10^{10} watt/cm^2 or 3.7×10^6 V/cm, is in rather good agreement with Maynard's[1] value of 4×10^{10} watt/cm^2 for a 50% larger focal radius but a slightly lower gas density.

Figure IV-7 shows calculated excitation and ionization frequencies per molecule for electrons in N_2 under conditions such that $\omega >> \nu_m$. These calculations were made using the cross sections and computational procedures discussed by Engelhardt and Phelps.[19] We have not calculated the excitation frequency, etc. for N_2 at atmospheric pressure since no measurements are available of the time of breakdown as a function of laser power. Without such data we cannot be sure of the significance of the observed threshold.[20] A preliminary attempt to compare theory and experiment is given in the next section.

D. Approximate Threshold Predictions

In this section we will make use of the excitation, ionization, and diffusion coefficients for He and N_2 which have been given in Ref. 1 and in the preceding section to predict approximate relations for the intensity required to produce breakdown of these gases by a pulsed ruby laser. We shall calculate the laser intensity necessary to satisfy two breakdown

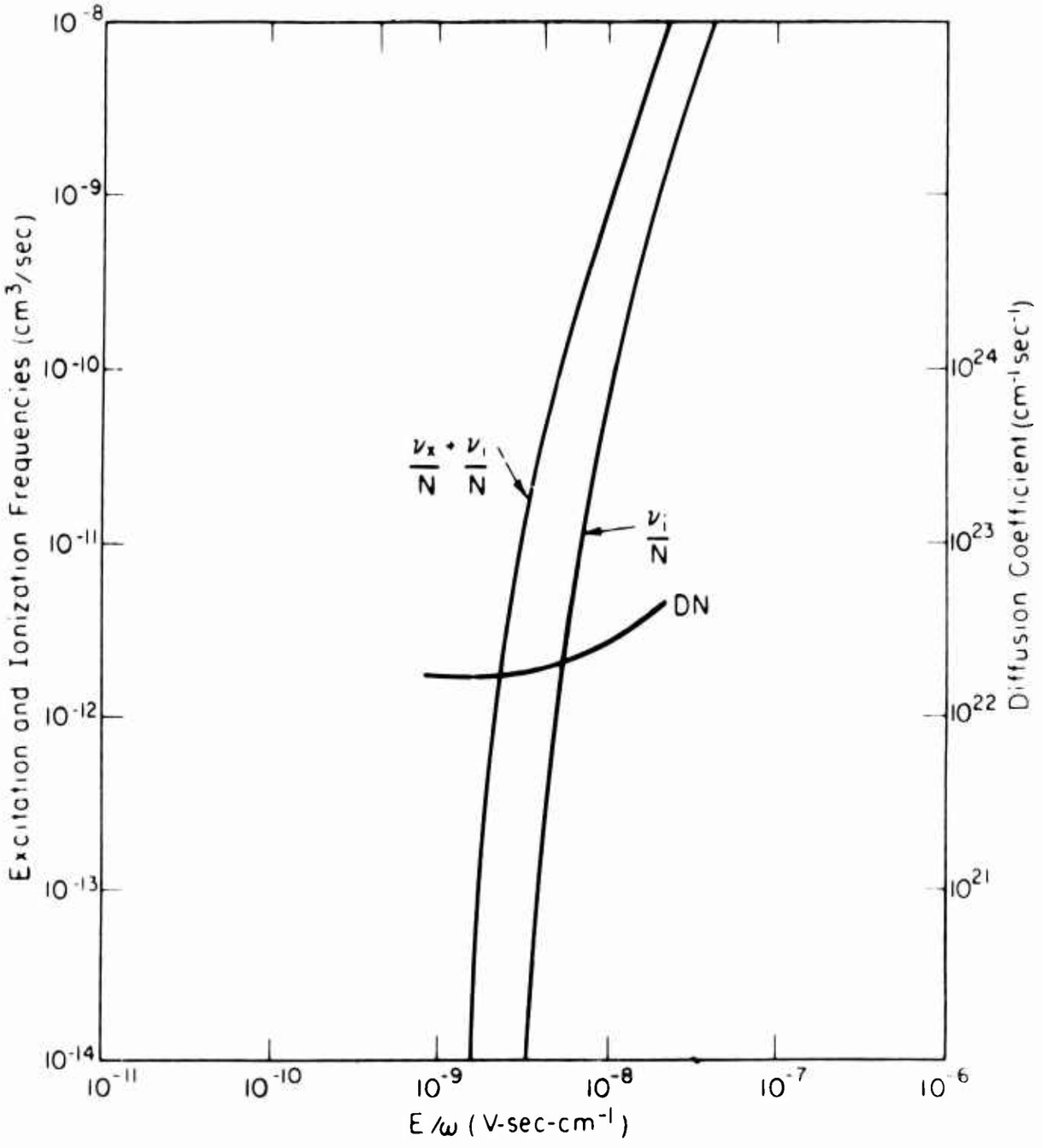

Figure IV - 7 **Electronic Excitation and Ionization in N_2 for $\omega >> \nu_m$**

criteria. First, we assume that the breakdown threshold is determined by the condition that the electron ionization frequency equal the free diffusion frequency. This static or diffusion controlled condition is the same as the conventional microwave breakdown criteria and has been applied by several authors [3] to the laser breakdown problem. Secondly, we assume that the breakdown threshold is determined by the requirement that the ionization increase from one electron in the focal volume to complete ionization during the time the laser pulse is on. In the results shown in Figures IV-8 and IV-9, we have continued to make the simplifying assumptions discussed in Ref. 1, e.g., a spatially uniform laser intensity, completely absorbing boundaries at the focal spot radius, a constant amplitude of laser intensity for the duration of the pulse, negligible effect due to electron attachment, and the presence of an initiating electron at the beginning of the laser pulse. It will be noted that we have not shown a limiting curve corresponding to the threshold laser intensity required to produce an initiating electron during the laser pulse. As indicated previously [2], one can predict the dependence of this minimum laser intensity only if one knows the nature and density of the atoms which supply the initiating electron. Attempts to measure this ionization rate experimentally [21] and to predict it theoretically have been unsuccessful. [22]

The static or diffusion controlled breakdown criteria is obtained by setting $\gamma = 0$ in Eq. (13) of Ref. 1 so that

$$\nu_x + \nu_i = \frac{D}{\Omega^2} \qquad (13)$$

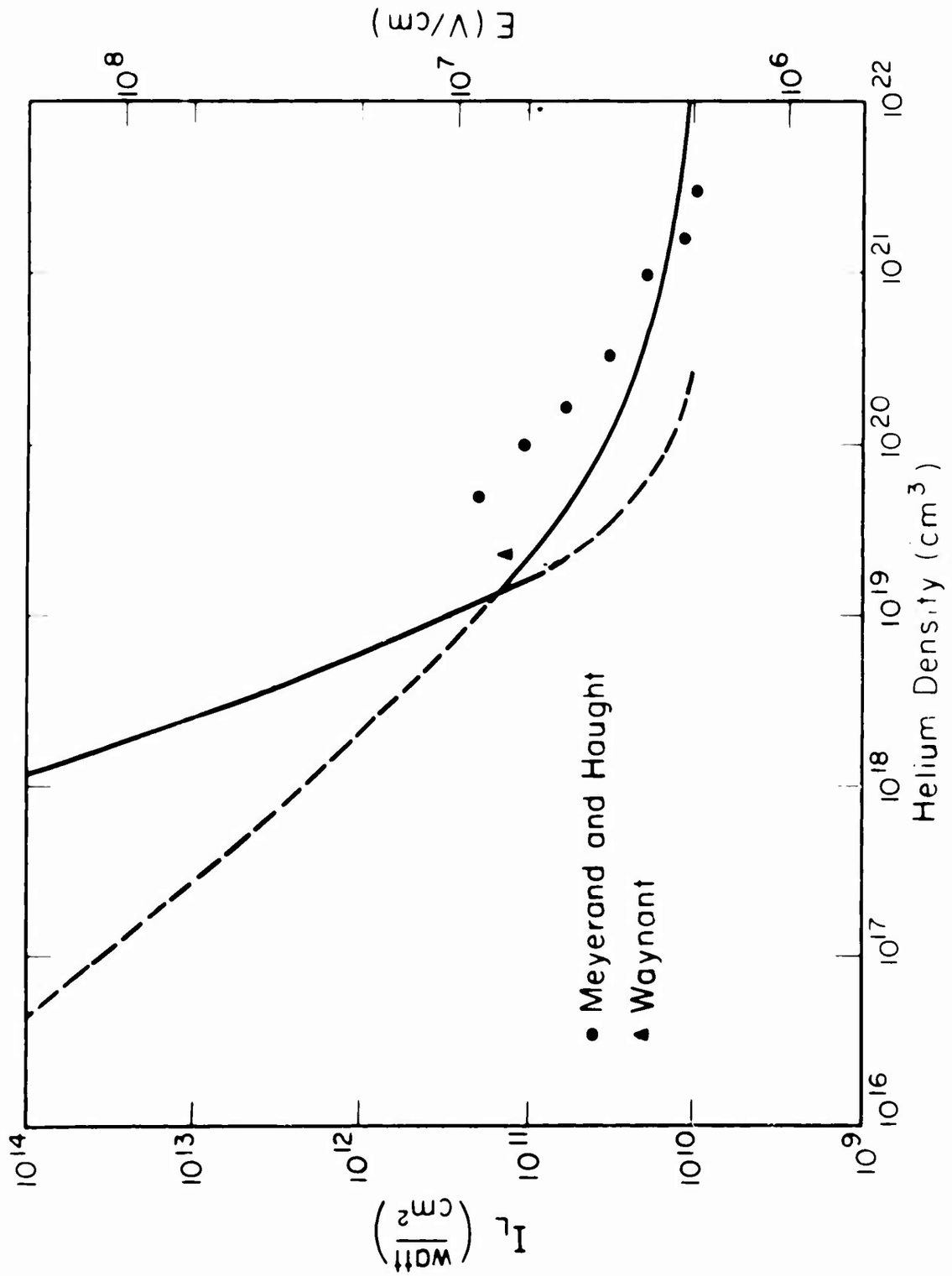

Figure IV - 8 **Laser Breakdown in He**

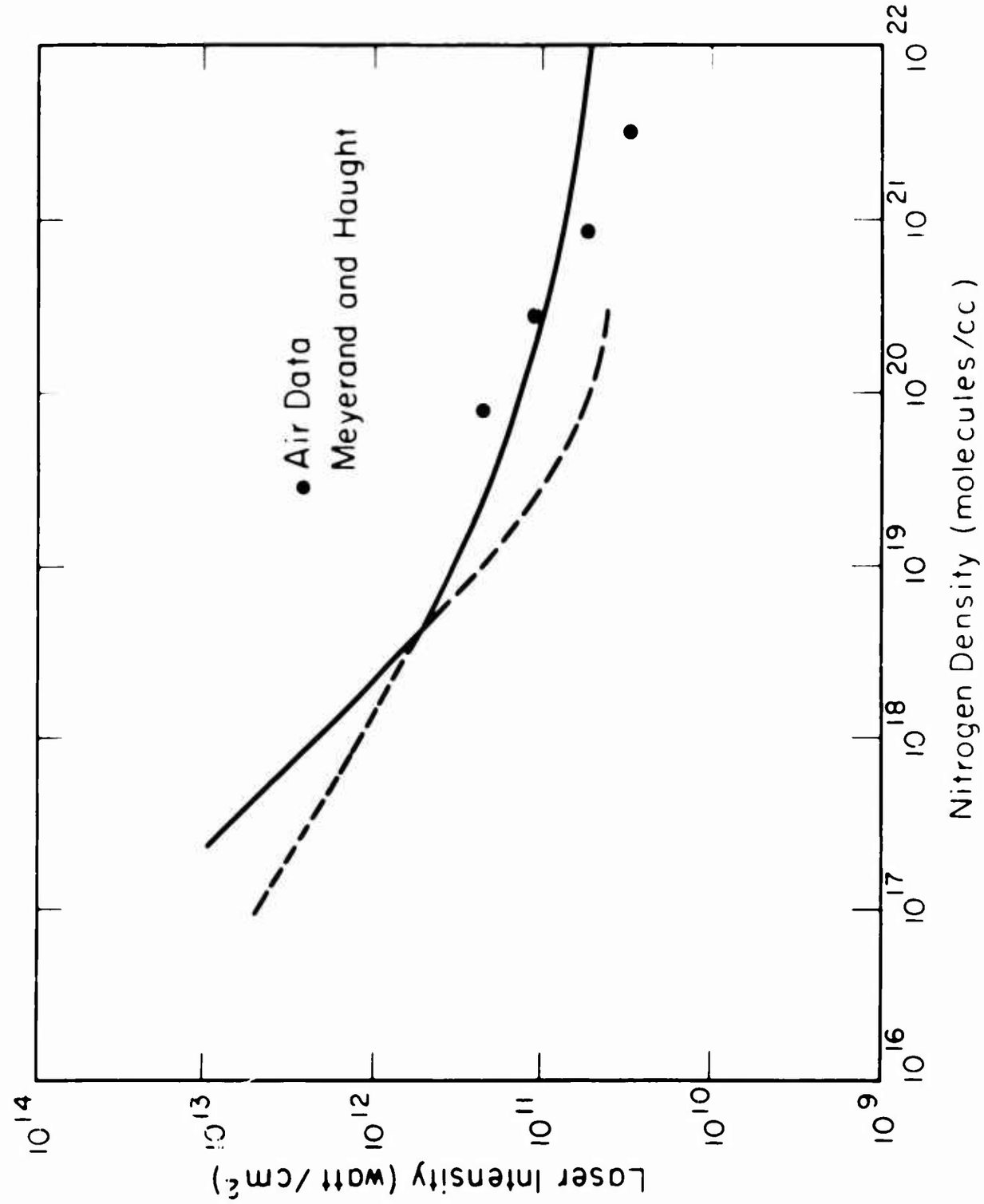

Figure IV - 9 Laser Breakdown Thresholds in N_2

Since $(\nu_x + \nu_i)/N$ and D/N are functions only of E/N and ω/N in the microwave theory used here, it is convenient to rewrite Eq. (13) in the form

$$\frac{(\nu_x + \nu_i)}{DN^2} = \frac{1}{N^2\Omega^2} \qquad (14)$$

Here $(\nu_x + \nu_i)/N^2$ corresponds to the usual ac ionization coefficient. When $\omega >> \nu_m$, the value of E/ω required for breakdown can be determined directly from a plot of $(\nu_x + \nu_i)/N^2$ vs E/ω. The steeper curves for Figures IV-8 and IV-9 show the result of such calculations for He and N_2 when R is taken to be 10^{-2} cm. The diffusion controlled threshold curve shown for N_2 is low by as much as 20% at the highest densities because the corrections due to a finite ω/ν_m had not been calculated at the time the graph was prepared.[23]

The threshold intensity required to satisfy the density buildup condition is calculated from Eq. (13) of Ref. 1 by neglecting the D/Ω^2 term and assuming that the electron density increases by e^{30} during a 60 nsec constant amplitude laser pulse. This relatively large value was used in order to approximate conditions in the experiments of Maynant[19] rather than those of Meyerand and Haught.[3] Thus, the threshold condition for the shallower curves of Figures IV-8 and IV-9 is

$$\frac{\nu_x + \nu_i}{N} = \frac{\gamma}{N} = \frac{5 \times 10^{8}}{N} \frac{cm^3}{sec} \qquad (15)$$

Again the curve shown for N_2 has not yet been corrected for finite ω/ν_m, and, in this case, is low by as much as a factor of 2 at the higher

densities.

We shall conclude this discussion with comments regarding the comparison of the experimental data and theoretical curves of Figures IV-8 and IV-9. First we note that the two threshold curves cross at gas densities somewhat below atmospheric so that diffusion losses determine the threshold at the lower gas densities and the buildup of electron density determines the threshold at the higher densities. These threshold determining curves are shown by solid lines. In the case of He, Figure IV-8 shows that this rough theory is in reasonable agreement with the data of Gaynant.[12] When consideration is given to the shorter laser pulse length used by Meyerand and Haught the agreement is reasonable at near atmospheric density but the theoretical curve seems to decrease too slowly with increasing gas densities N. It is to be noted that the relative values of the breakdown threshold in He given by Minck[3] are similar to those of Meyerand and Haught in Figure IV-8.

Figure IV-9 shows a comparison of the approximate theoretical threshold laser intensities for N_2 with the experimental data of Meyerand and Haught.[3] This comparison is reasonable from the point of view of the microwave theory since the measured Townsend ionization coefficient for N_2 and air are nearly the same[24] and their diffusion coefficients are expected to be similar. As in the case of helium the agreement is quite good at the lower gas densities when one considers the shorter pulse length used by Meyerand and Haught. The relatively rapid decrease in experimental threshold laser intensity with increasing gas density compared to the theoretical curve is similar to that shown in Figure IV-8 for He.

This behavior is also seen in the relative values given by Minck.[3] The finite ω/ν_m correction referred to would increase the discrepancy even further at high gas densities. In both He and N_2 it would appear that the decrease in the efficiency of conversion of photon energy into excitation (and ionization) predicted by the microwave theory at low E/ω is too large. In the He case this energy goes into elastic recoil collisions while in the N_2 case this energy results in the excitation of relatively high vibrational states.[19] Obviously, further investigations of this behavior are necessary.

E. Summary

This report presents evidence that the absorption of relatively high energy photons in free-free transitions may in some cases lead to small ($\sim$ 30%) but possibly significant deviations in the rate of growth of an electron avalanche from that predicted by an appropriate extension of the microwave theory, i.e., the continuous form of the Boltzmann equation. This evidence is obtained by solving the difference form of the Boltzmann equation in both the steady state and time dependent cases for various simple models of the electron-atom or electron-ion collision processes. However, since direction and magnitude of the deviation depend upon the model used and since several important affects are not included further comparisons of the two theories are desirable.

The report also presents additional calculations of the excitation, ionization, and diffusion coefficients and makes use of these to compute avalanche growth times and approximate curves of the laser intensity required for breakdown as a function of gas density. In general the agreement between theory and experiment is within a factor of 2 in laser

intensity or 40% in laser electric field intensity. There are, however, systematic deviations between theory and experiment which should be explored further.

V. REFERENCES

1. A. V. Phelps, Westinghouse Research Report 64-1E2-1113-R1. This will be referred to as Reference 1 (included in Theoretical Investigations in First Interim Technical Documentary Report , August 1964).
2. A. V. Phelps, Research Memo 64-1E2-1113-M1 (Appendix A).
3. See for example R. G. Meyerand and A. F. Haught, Phys. Rev. Letters 11, 401 (1963) and 13, 7 (1964); R. W. Minck, Jour. Appl. Phys. 35, 252 (1964); and J. K. Wright, Proc. Phys. Soc. 84 41 (1964).
4. F. T. Byrne (private communication).
5. D. P. Gaver and J. A. Marshall, Westinghouse Research Report 64-1E0-113-R1. Our form of Eq (5) is somewhat different from that of this report because of the inclusion of the presence of electrons of zero energy (Appendix B).
6. Equation (1) can be obtained from Eq (6) of Reference 1 by assuming that $f(\varepsilon)$ is a series of impulse functions $\delta(\varepsilon - i\hbar\gamma)$, centered at $i\hbar\gamma$, such that $\varepsilon^{1/2} f(\varepsilon) d\varepsilon = P_i \delta(\varepsilon - i\hbar\gamma)$ and $\Sigma P_i = 1$.
7. T. Holstein (private communication).
8. W. P. Allis, Handbuch der physik, edited by S. Flugge (Springer-Verlag, Berlin, 1956), Vol. 21.
9. This technique used in this analysis can easily be extended to the case of an absorption frequency with an arbitrary energy dependence.
10. C. L. Chen, Phys. Rev. 135, A627 (1964). A similar result for the frequency of absorption collisions is well known in the theory of astrophysical processes. See for example L. Spitzer, Physics of Fully Ionized Gases (Interscience Publishers, Inc., New York 1956) p. 89. Note that we have neglected the energy variation of the logarithmic term.

11. A. F. Haught (private communication) has indicated that he is conducting a similar investigation.

12. Because of uncertainties regarding the photon absorption frequency at low electron energies several other approximations to the low energy behavior but having the same dependence at high energies have been tried. In every case the excitation frequency calculated using the discrete model for electron-neutral collisions was lower than that calculated using the continuous model.

13. Here again an arbitrary energy dependence for a single excitation process would not add any significant complication.

14. The effect of elastic collisions is included in the microwave theory and has been considered in the laser breakdown problem by J. K. Wright, Proc. Phys. Soc. 84, 41 (1964). An approximate treatment has been developed in connection with our statistical solution and shows that elastic collisions cannot be neglected in the present problem.

15. A further point of interest is that by slightly modifying our relation between ε and i we can regard the solutions given here as numerical solutions to the continuous form of the time dependent Boltzmann quation. In this case $h\gamma$ is chosen as small as possible consistent with computer limitations.

16. This effect can be taken into account in the Boltzmann equation by adding terms corresponding to the production and loss of electrons as is often done in the theory of microwave breakdown[8]. This procedure would considerably increase the amount of computer time required but may eventually prove worthwhile.

17. A. G. Engelhardt and A. V. Phelps, Phys. Rev. 133, A375 (1964). The excitation and ionization frequencies calculated using this excitation cross section may be somewhat in error since similar calculations for $\omega = o$ disagreed with the available experimental ionization coefficients by as much as a factor of two. The error in the excitation frequency is probably much less than in the ionization frequency because essentially all of the electron energy is dissipated in excitation collisions.

18. R. Waynant, this interim report on Contract AF30(602)3332. Pages 17,19,22.

19. A. G. Engelhardt and A. V. Phelps, Phys. Rev. 135, A1566 (1964).

20. The uncertainty as to the significance of the observed threshold, i.e., the minimum laser power density at which light output, light absorption or charge production is observed, is especially pronounced in He where Waynant's data[18] shows that there is little increase in the time of breakdown as the laser power density is increased. This is in contrast to the predictions of Figure IV-4 of Reference 1. One is tempted to propose that in this case the threshold is determined by the "threshold" for the production of an initiating electron.[2] However, preliminary experiments[18] in which Hg vapor was added to the helium do not support this hypothesis. Further studies are desirable but probably cannot be made on this contract because of time and money limitations.

21. As reported elsewhere,[18] an unsuccessful attempt was made to measure the ionization produced by a pulsed ruby laser in mercury vapor at pressures of the order of 4×10^{-3} torr. Laser induced ionization of various gases has been reported by E. K. Damon and R. K. Tomlinson, Applied Optics 2, 546 (1963). However, Tomlinson now states (private communication) that attempts to repeat these experiments have also been unsuccessful.

22. Recently F. V. Bunkin and A. M. Prokhorov, J. Exptl. Theoret. Phys. 46, 1090 (1964), Translation; Soviet Physics JEPT 19 739 (1964), have considered the ionization of atoms by the tunneling process in a high intensity radiation field. Their results also show that this process is negligible under conditions of interest to us.

23. The effect of finite ω/ν_m is more difficult to compute in N_2 and Ar than in He because the approximation that $\nu_m(\mathcal{E})$ is independent of collision frequency is not valid for these gases. This correction is important only at the highest gas densities considered.

24. A. Von Engel, Handbuch der Physik, edited by S. Flugge (Springer-Verlag, Berlin, 1956) p. 534.

APPENDIX A

SOME CONSEQUENCES OF LASER BREAKDOWN INITIATION BY A NON-LINEAR PROCESS

A. V. Phelps
Westinghouse Research Laboratories
Pittsburgh 35, Pennsylvania

The model of the laser breakdown process which appears to best fit the presently available data is that in which the initiating electron is produced by non-linear or multiphoton ionization of an impurity or the main gas and is followed by an exponential growth of ionization resulting from either electron excitation followed by photoionization or direct ionization by electron impact.[1] The purpose of this memorandum is to examine some of the consequences of the assumption that a non-linear or multiphoton process provides the initial electron.

1) Time dependence of ionization

The time dependence of the ionization resulting from a process in which the photon flux acts directly on the neutral atoms is significantly different from that in which free electrons absorb the photon energy and produce ionization. The continuity equation for the electron density, n, in the general case is

$$\frac{\partial n}{\partial t} = \alpha M + \nu_{xi} n - D\nabla^2 n , \qquad (1)$$

where α is the rate of ionization of neutral atoms or molecules of density M, ν_{xi} is either the frequency of excitation and ionization by electron impact,[1] and D is the electron diffusion coefficient. Unless otherwise stated, we will assume that the laser power increases abruptly to some constant value at t = 0, so the

α, ν_{xi}, and D are constants. As before, we approximate the solution to this equation by replacing $D\nabla^2 n$ by Dn/Λ^2 where Λ is the diffusion length corresponding to the fundamental mode in a cylinder with a radius equal to that of the focal spot. Equation (1) now reduces to

$$\frac{dn}{dt} = \alpha M + (\nu_{xi} - \nu_D) n \qquad (2)$$

where $\nu_D = D/\Lambda^2$. The solution to this equation for the case of $n = 0$ at $t = 0$ and $n \ll M$ is

$$n = \frac{\alpha M}{(\nu_D - \nu_{xi})} [1 - \exp (\nu_{xi} - \nu_D) t] . \qquad (3)$$

For $\nu_{xi} < \nu_D$, this solution reaches a steady state value of $\alpha M (\nu_D - \nu_{xi})^{-1}$, whereas for $\nu_{xi} > \nu_D$ it increases exponentially with a growth constant of $\nu_{xi} - \nu_D$. For $\nu_{xi} - \nu_D = 0$, $n = \alpha M t$. Note that our assumption of $n \ll M$ may be violated at rather low n, if M is an impurity.

The mathematical approach which is used above does not show the possible discontinuous nature of the true breakdown problem, i.e., Eqs. (1) - (3) are valid only when there is a reasonably large number (e.g., 10 or more) of electrons present. This point is important in evaluating experimental data since it means that if the rate of electron production by the non-linear process is small enough it will determine the minimum laser power at which breakdown is normally observed.[2] Thus, if the effective pulse length is Δt and if $\alpha M \Delta t < 1$, then even though $(\nu_{i,x} - \nu_D) \Delta t > \ln (10^{19}/10^5)$ so that an avalanche could ionize essentially all of the atoms, breakdown may not occur. If this were the case breakdown might occasionally be observed at laser powers significantly below that for which $\alpha M \Delta t \sim 1$, i.e., breakdown might be initiated by the truly random background electron. The occurrence of a single rare breakdown event at power levels well below the normal threshold has been observed.[3]

If the production of an electron by a non-linear process does effectively determine the threshold, then observations of the time dependence of the growth of ionization and excitation should show that growth constant

$\gamma = \nu_{x,i} - \nu_D$ does not approach zero as the breakdown threshold is approached but that the observed delay is due to a delay in the time of initiation of the avalanche. Since it now appears[1] likely that measurements of the light intensity will follow the ionization build up, it may be possible to extrapolate measurements of the ionization growth back to the time of appearance of the initiating electron. Such measurements will require the use of photodetectors with sufficient sensitivity and speed to measure the light generated during the portion of the growth period when the degree of ionization of the gas is small, e.g., when the light output is $\sim$1% or less of the peak value.

2) Dependence of ionization on geometry, laser power, etc.

The requirement that the laser produce the initiating electron means that in general two distinct threshold conditions must be met. These two conditions will have rather different dependences on laser power, focal spot size, gas density, and laser frequency. The dependence of the avalanche growth condition on the experimental parameters has been discussed in detail for helium[1] using the microwave theory as a basis for obtaining quantitative predictions. In general, this analysis shows that the threshold condition for gas densities of the order of atmospheric and reasonably small focal spot radii is determined by balancing an effective ionization frequency which varies approximately as $N(E/\omega)^n$, $n=2$ to 5 against a diffusion frequency which varies approximately as $(NR^2)^{-1}$. Thus, the avalanche threshold condition is that $(NR)^2(E/\omega)^n$ is a constant depending upon the gas. In terms of the laser power required for threshold, $P \propto R^2E^2$, so that $P \propto N^{-4/n} R^{2-4/n} \omega^2$.

The exact dependence of the non-linear or multiphoton initiation threshold on experimental parameters varies with the theoretical description of the ionization process which is most appropriate to the gas under consideration Thus, the ionization may occur due to tunneling of an electron out of the atom through the potential barrier created by the intense applied field.[4] Neglecting the fact that the electric field is alternating, the frequency of field induced ionization events per atom is given approximately[5] by

$$\alpha = \nu_e \exp(-6.8 \times 10^7 I^{3/2} E^{-1})$$

where ν_e is the effective frequency at which electrons approach the potential barrier and is roughly 10^{16} sec^{-1}, I is the ionization potential of the atom and E is the electric field strength. For typical laser breakdown conditions I = 15.8 eV and E = 10^7 V/cm so that $\alpha = 10^{-426}$ cm^3/sec. Therefore field strengths of the order of 5×10^8 V/cm would be required to produce significant ionization. This crude calculation would seem to indicate that a multiphoton process is involved.

The ionization coefficient per atom according to the multiphoton theory is expected to be proportional to $(F)^m$ where F is the laser photon flux and $m \geq (I/h\nu)$. For argon and a ruby laser m = 9, so that the requirement that $\alpha M\Delta t \approx 1$ means that the threshold condition would require that $E^{18} M\Delta t$ be a constant or that the threshold power obey the relation $P\alpha (M\Delta t)^{-0.11} R^2$. If the gas ionized by the multiphoton process were mercury (I = 10.4 eV), we would expect $P\alpha (M\Delta t)^{-0.17} R^2$, and that the power required would be very much lower. According to these relations the power required to meet this threshold condition should be insensitive to changes in the gas density and should increase with the square of the focal spot size. This means that the multiphoton process threshold condition will become more difficult to meet relative to the avalanche threshold condition as the focal radius is increased. This should lead to a greater spread in the breakdown time.

The difference in behavior of the two ionization processes is most pronounced when the integrated laser energy is fixed and the spatial distribution of the focus is varied, either intentionally or by accident as when the laser mode pattern changes. Thus a 20% increase in the peak laser power at any point in space will increase the ionization rate due to the multiphoton process by factors of from 3 for mercury to 5.1 for argon whereas the ionization frequency due to the avalanche process increases only by a factor of about 1.6. This high sensitivity of the multiphoton, or other non-linear, ionization to the intensity of the laser power may account for some of the observed fluctuation in the breakdown time. If this effect is important at a fixed laser pulse energy, the

shorter breakdown times should correspond to those pulses in which the laser power distribution is more sharply peaked in the focal region whereas the longest breakdown times would correspond to pulses in which the spatial variation in laser power was relatively uniform. Experimental data may be available for checking this hypothesis.[3] An alternative explanation of the observed spread in breakdown times is given in the next section.

3) Statistics of Breakdown

In this section we consider more explicitly the effects of a non-linear initiation mechanism on the statistics of breakdown. Our main point is that the theory is essentially no different from that applicable in the case of Townsend breakdown when the initiating electron is produced by a constant external source but with the condition that the probability of producing an avalanche is a function of the field strength or in the case in which the initiating electrons are produced by field emission from a cathode. These problems have been considered previously by Phelps and Berg[6] and others. This theory is especially simple when the time required for the avalanche to grow to the value required for observation of breakdown is negligible. In this case the probability of breakdown G(t) after a time t is given by

$$\ell n\, G(t) = -\int_0^t \lambda(t)\, dt \qquad (4)$$

where $\lambda(t)$ is the frequency of production of electrons capable of initiating the avalanche. According to the laser breakdown model being discussed we expect $\lambda(t)$ to be proportional to $ME^{2m}(t)$, i.e., a very rapidly varying function of time. The probability that breakdown will be observed at a time between t and t + dt is found by differentiating Eq. (4) to get

$$dG = -\lambda(t)\, G(t)\, dt \qquad (5)$$

This is actually the basic equation for G(t). As shown by Phelps and Berg,[6] Eq. (5) can be used to evaluate $\lambda(t)$. Thus,

$$\lambda(t) = - \frac{1}{G(t)} \frac{dG}{dt} \tag{6}$$

The behavior of the various functions defined above is shown in Fig. 1. Here we have shown, in Fig. 1a, the time dependence of the laser power, P(t), from an oscilloscope photograph taken by Waynant.[7] Also shown in Fig. 1a are the relative values of $\lambda(t)$ as calculated for multiphoton ionization of helium (m = 11) and of mercury (m = 6). Figure 1b shows curves of G(t) as calculated from the $\lambda(t)$ for m = 11 with the magnitude of $\lambda(t)$ adjusted so as to produce an average number of electrons per pulse, N, of 1, 5, 18, or 2050. Here $N = \ell n\, G(\infty) = \int_0^\infty \lambda(t)dt$. The corresponding values of dG/dt are shown in Fig. 1c. The most striking feature of these curves is the relatively small region of time, e.g., 5-10 nsec halfwidth, over which the initiating electrons are produced with an appreciable probability. This is consistent with an apparent upper limit to the observed breakdown times. A second feature of these curves is the small but definite shift of the curve of the probability of initiation, Fig. 1c, to shorter times as the peak laser power is increased. With m = 11 the increase in N from 1 to 5.18 and 2050 represents an increase in peak laser power by factors of 1.16 and 2.0, respectively. If the time required for avalanche growth were negligible then the factor of two increase in laser power would result in breakdown at times of the order of one half the time required to reach peak power.

If our assumption that the time required for avalanche growth is negligible and if fluctuations in the spatial distribution of the laser intensity can be neglected, then a plot of the number of breakdown events per unit time should resemble Fig. 1c. The data obtained for argon by Waynant[3] show only at the higher laser energies are the distributions similar to Fig. 1c. The data obtained at energies nearer threshold yields distributions which are considerably more spread out in time and for which the peak occurs much later

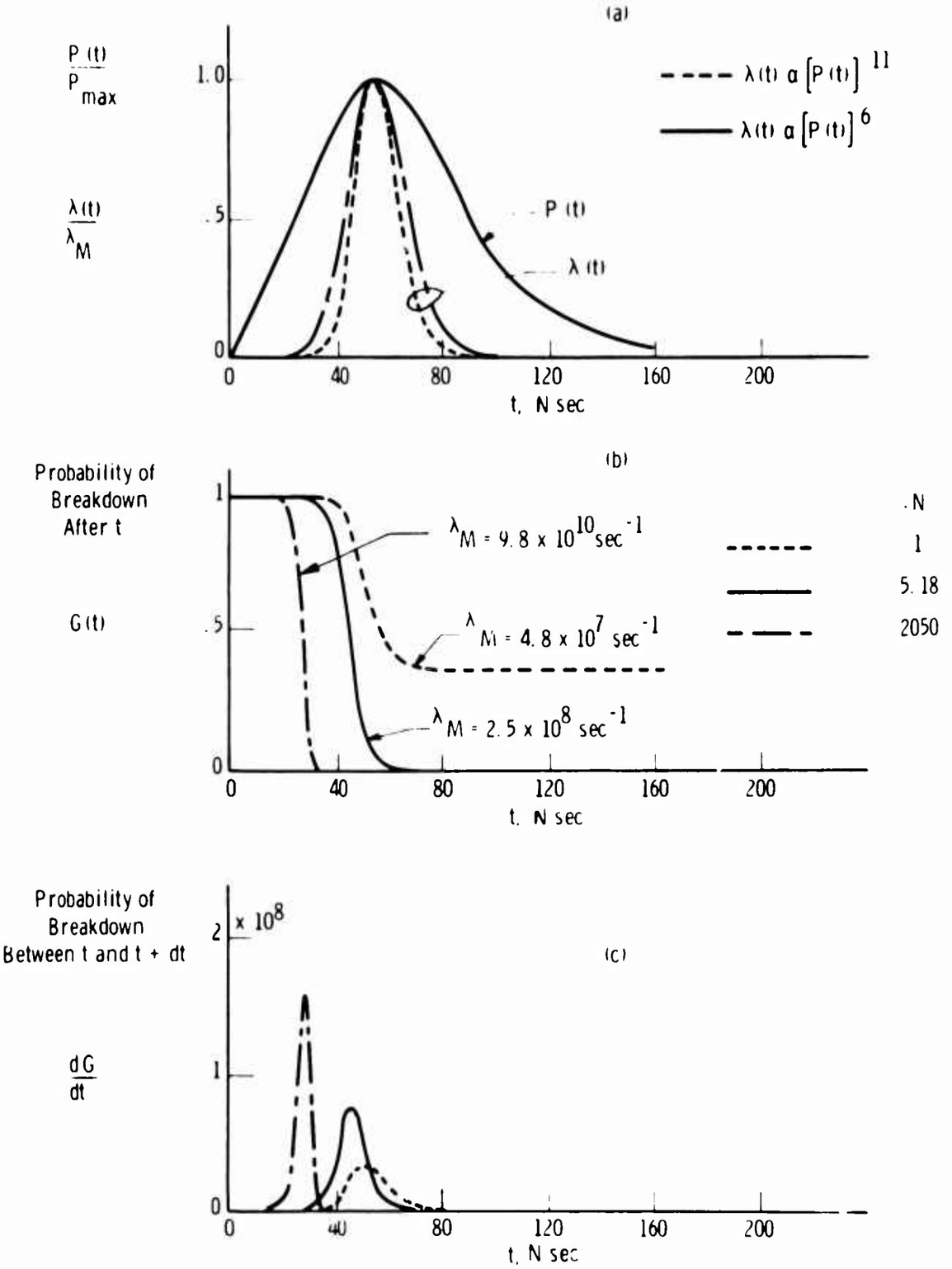

Fig. 1—Calculations of the probability of laser breakdown with non-linear ionization initiation mechanism

in time. The shift to later times at lower laser energies is characteristic of longer avalanche growth constants and suggests strongly that the avalanche growth time is not negligible. If the laser power were constant during the growth, then the finite growth time could be taken into account at a fixed laser energy simply by shifting the time scale in Figs. 1b and 1c by an appropriate amount. With a time varying laser power there will be a tendency for the cases in which the initiating electron occurs later to have a lower average growth constant. However, at present this effect seems too small to produce the observed spread. Obviously, further investigation of this area is desirable.

d) Conclusions

The arguments presented in this report indicate that the non-linear mechanism which probably provides the initiating electron for laser breakdown is multiphoton absorption. This process produces electrons only over a relatively narrow time interval and so its effect is consistent with the tendency of the breakdown time to show an upper limit when plotted as a function of laser power. The time required for avalanche growth appears to become appreciable as the laser energy is reduced toward threshold in argon at 1 atmosphere.

References

1. This model is discussed in some detail in Research Report 64-1E2-113-R1. It is essentially the same model as proposed earlier for atomic hydrogen by P. Browne in Scientific Paper 64-814-259-P1, and by J. K. Wright, Proc. Phys. Soc. 84, 41 (1964).

2. We note that while it is possible that the ionization produced by the non-linear process could be sufficient to produce all of the observed breakdown effects, it does not seem likely that this is the case unless the ionization potential of the gas is quite low.

3. R. Waynant (private communication).

4. This process is being studied in further detail by M. Mizushima.

5. R. Gomer, Field Emission and Field Ionization (Harvard University Press, Cambridge, Mass. 1961), p. 70.

6. A. V. Phelps and D. Berg, Westinghouse Research Report 6-94439-6-R4, May 1958.

7. R. W. Waynant, Appendix B of the proposal for PR64-431

APPENDIX B

A RANDOM WALK PROBLEM IN LASER PHYSICS

D. P. Gaver, J. A. Marshall

Introduction

This report describes some preliminary work on probability models in physics, carried out at the request of Dr. A. Phelps. The results and methods discussed provide a convenient starting point for checking certain calculations and models used by physicists; in particular, some easily manipulated "continuous" approximations may be appraised for numerical accuracy.

The write-up to follow is in the nature of a progress report. More work along lines similar to that described here, can be conducted.

A First Model

A particle (electron) executes a random walk in continuous time over a denumerable set of (energy) states 1, 2, 3, ... Steps in the walk (energy changes) occur at random times because of interaction with particles of another class (photons); the steps are either up by one unit, i.e. from state i to i+1, or down by one unit, i.e. from i to i-1, except that when the lowest state, 1, is reached no further down-jumps are possible. Furthermore, when some sufficiently high state, H, is reached the particle jumps instantaneously back to state 1, and the walk begins again. In fact, when the jump from H to 1 occurs, another particle is born and occupies state 1 at birth, thereafter walking independently of the first. This process then continues indefinitely.

In this report we study the probability distribution of the random variable T_{1H}, described as the time of a particle's first passage to state H, having started at state 1. In particular we compare the mean, or expected, first passage times, $E(T_{1H})$, as the latter are computed using various hypotheses about jump probabilities. We also discuss the problem of continuous approximation of the path of the particle through energy space.

In order to obtain explicit expressions for $E(T_{1H})$ we make the specific assumption that the particle walk is a time-homogeneous birth-and-death process, i.e. that the probability that a particle, currently occupying (energy) state i ($i \geq 1$) jumps to state i+1 in the time dt is $\lambda_i dt + o(dt)$; the corresponding down-jump probability is $\mu_i dt + o(dt)$, except that $\mu_1 = 0$; importantly, too, all jump probabilities are influenced only by present state, and not by any previous history. This makes the walk a simple Markov process. Both λ_i and μ_i are positive and independent of the time during which the process has gone on. An introduction to such processes will be found in Feller [2]. The above assumptions imply that the distribution of the sojourn time, S_i, of a particle in a particular state, i, i.e. the uninterrupted time from an entrance into i until the next exit therefrom, is distributed exponentially

$$\text{Prob}[S_i \leq t] = 1 - e^{-(\lambda_i+\mu_i)t} . \qquad (1)$$

If, for some reason, the exponential distribution is physically implausible the distribution (1) can actually be made of arbitrary form, leading us to the class of semi-Markov rather than Markov processes. The methods to be

described then need only be altered trivially to obtain explicit solutions, provided there is independence between the successive sojourns. Independence would not occur, for example, if the event that a particle had just entered state i from below, i.e. from i-1, were to shorten the time of sojourn of the particle in S_i, or perhaps alter the probability with which the particle jumps from i to i+1 or to i-1. Such effects might derive from considerations of velocity as well as position; we rule them out.

Under our assumptions, a convenient way of computing the Laplace-Stieltjes transform $E(e^{-sT_{1H}})$, the expected first passage time, $E(T_{1H})$, and higher moments as well has been given in Gaver [3]; formulas for $E(T_{1H})$ have been given previously by others. We will not utilize the L.-S. transform here, although by employing this function it should be possible to prove certain probability limit theorems of use when the second stage of the problem -- involving particle branching when jumps from high energy states to state 1 -- is attacked. From [3]: let A_i denote the first passage time from state i to i+1 (i.e., the elapsed time from first entrance into state i to first entrance into state i+1). Then if

$$a_i(s) = E(e^{-sA_i}) , \tag{2}$$

$$a_i(s) = \frac{\lambda_i}{s+\lambda_i+\mu_i\left\{1-a_{i-1}(s)\right\}} ; \tag{3}$$

since initially

$$a_1(s) = \frac{\lambda_1}{\lambda_1+s}$$

we can successively substitute to obtain $a_i(s)$ for any i. Finally, because

$$T_{1H} = A_1 + A_2 + \ldots + A_{H-1} \tag{4}$$

with $\{A_i\}$ a sequence of independent random variables we find

$$E(e^{-sT_{1H}}) = \prod_{i=1}^{H-1} a_i(s). \tag{5}$$

For the expectation or mean of T_{1H} we use the fact that

$$E(T_{1H}) = \sum_{i=1}^{H-1} E(A_i)$$

and the recursion formula, derivable from (3) by evaluating its derivative with respect to s at s = 0,

$$E(A_i) = \frac{1}{\lambda_i} [1 + \mu_i E(A_{i-1})], \tag{6}$$

which in turn gives

$$E(A_i) = \frac{1}{\lambda_i} + \frac{\mu_i}{\lambda_i}\frac{1}{\lambda_{i-1}} + \frac{\mu_i\mu_{i-1}}{\lambda_i\lambda_{i-1}}\frac{1}{\lambda_{i-2}} + \ldots + \frac{\mu_i\mu_{i-1}\cdots\mu_2}{\lambda_i\lambda_{i-1}\cdots\lambda_2}\frac{1}{\lambda_1}. \tag{7}$$

It is expression (7) that will be particularly discussed in what follows. Note that the expression (6) can be easily evaluated by computer, for it is a simple recursion formula. This has been carried out in certain cases, believed to be of interest in applications; some examples will follow. First we present some special cases that may be of use.

Special Case I: $\lambda_i=\lambda$, $\mu_i=\mu$ (i=1,2,...; but $\mu_1=0$).

In this walk the probabilities of jumps and the jump rates (hence sojourn times) do not depend upon the states. From (6) or (7) we easily get

$$E(A_i) = \frac{1}{\lambda} \frac{1 - (\frac{\mu}{\lambda})^i}{1 - \frac{\mu}{\lambda}} \qquad \text{for} \quad \mu \neq \lambda$$
$$= \frac{i}{\lambda} \qquad \text{for} \quad \mu = \lambda. \tag{8}$$

and therefrom

$$E(T_{1H}) = \frac{H-1}{\lambda-\mu} - \frac{\mu}{(\lambda-\mu)^2} [1 - (\frac{\mu}{\lambda})^{H-1}] \qquad \text{for } \lambda \neq \mu$$
$$= \frac{H(H-1)}{2\lambda} \qquad \text{for } \lambda = \mu. \tag{9}$$

For large H we can put, for the case $\lambda \neq \mu$,

$$E(T_{1H}) \sim \frac{H}{\lambda-\mu} - \frac{\lambda}{(\lambda-\mu)^2} \qquad \text{for } \mu = \lambda$$
$$\sim (\frac{\mu}{\lambda})^{H-1} \frac{\mu}{(\lambda-\mu)^2} \qquad \text{for } \mu > \lambda \tag{9'}$$

where the approximation improves as H increases.

Special Case II: $\lambda_i = i\lambda$, $\mu_i = i\mu$ ($i=1,2,\ldots$; but $\mu_j = 0$).

In this model activity increases with energy. Again using (6) or (7) we get

$$E(A_i) = \frac{1}{A} \sum_{j=1}^{i} (\frac{\mu}{\lambda})^{i-j} \frac{1}{j} = \frac{1}{\lambda}(\frac{\mu}{\lambda})^i \sum_{j=1}^{i} (\frac{\lambda}{\mu})^j \frac{1}{j} \tag{10}$$

If $\lambda = \mu$ then the above series becomes the harmonic, and

$$E(A_i) \sim \frac{1}{\lambda} \ln i. \tag{11}$$

Therefore

$$E(T_{1H}) = \sum_{i=1}^{H-1} E(A_i) \sim \frac{1}{\lambda} \int_1^{H-1} \ln x \, dx \tag{12}$$

$$= \frac{1}{\lambda}[(H-1) \ln (H-1) - (H-2)]$$

where the approximation improves as H increases. We will not stop to write down the approximations obtainable for $\lambda \neq \mu$; these could be gotten by replacing the sums by integrals, perhaps in a refined form by use of the Euler-Maclaurin sum formula.

The above models have taken no account of a necessary physical restriction on the $\{\lambda_i\}$ and $\{\mu_i\}$ sequences imposed by "detailed balance". This principle requires that the transition rates for cases I and II be modified:

$$\underline{\text{Case I'}}: \quad \lambda_i = \lambda, \ \mu_i = \lambda \sqrt{\frac{i-1}{i}} \tag{13}$$

$$\underline{\text{Case II'}}: \ \lambda_i = i\lambda, \ \mu_i = (i-1)\lambda \sqrt{\frac{i-1}{i}} \ . \tag{14}$$

Notice that for large i we are very nearly in the cases I and II, with $\lambda = \mu$. However inclusion of detailed balance has the effect of slightly <u>decreasing</u> μ_i compared to its corresponding value in cases I and II, and hence <u>decreasing</u> $E(T_{1H})$.

Computations were carried out for cases I' and II' in order to compare the results of the continuous model with those of the discrete model developed above. Using (13) and (7) we find

$$E(A_i) = \frac{1}{\lambda} \frac{1}{\sqrt{i}} [\sqrt{1} + \sqrt{2} + \sqrt{3} + \ldots + \sqrt{i-1} + \sqrt{i}] \tag{15}$$

for case I' while (14) and (7) give 1/i times this result for case II'. Values of the quantity $F(T_{1H})$ were calculated for all values of H from 2 to 31 for each of the two cases (with $\lambda = 1$).

The corresponding results from the continuous model are

Case I': $E(T_{1H}) = (H-1)^2/3$, and

Case II': $E(T_{1H}) = 2(H-1)/3$.

Table 1 gives the results of the computations for the discrete model and compares these with continuous model, for the two cases. The agreement between the two models is seen to improve as H increases. Notice that the discrete model always gives the longer first passage times. As a check on this, consider approximating the discrete model by another one with smaller step size.

If we want to approximate the behavior of the particle over the original state space by a particle "walking" on a new state space which has smaller step size, we must find the appropriate values for the new parameters. If we take the original step size as 1 and the original parameters as λ_i and μ_i and the new step size as Δ with parameters $\lambda'_{i'}$ and $\mu'_{i'}$, then quantum mechanics suggests for

Case I': $\lambda'_{i'} = \left(\frac{1}{\Delta}\right)^2 \lambda$, and

$$\mu'_{i'} = \lambda'_{i'} \sqrt{\frac{i'-1}{i'}} ,$$

while for

Case II': $\lambda'_{i'} = i'\left(\frac{1}{\Delta}\right)\lambda$, and

$$\mu'_{i'} = \lambda'_{i'}(i'-1) \sqrt{\frac{i'-1}{i'}} .$$

Table 1

Values of $E(T_{1H})$ for the Discrete and Continuous Models and the Ratio of These Quantities for Cases I' and II' with $\lambda = 1$.

	Case I'			Case II'		
H	Discrete	Continuous	D/C	Discrete	Continuous	D/C
2	1.000	.33	3.00	1.000	.67	1.50
3	2.707	1.33	2.03	1.854	1.33	1.39
4	5.101	3.00	1.70	2.652	2.00	1.33
5	8.174	5.33	1.53	3.420	2.67	1.28
6	11.923	8.33	1.43	4.170	3.33	1.25
7	16.345	12.00	1.36	4.907	4.00	1.23
8	21.439	16.33	1.31	5.634	4.67	1.21
9	27.204	21.33	1.28	6.355	5.33	1.19
10	33.639	27.00	1.25	7.070	6.00	1.18
11	40.744	33.33	1.22	7.780	6.67	1.17
12	48.519	40.33	1.20	8.487	7.33	1.16
13	56.962	48.00	1.19	9.191	8.00	1.15
14	66.074	56.33	1.17	9.892	8.67	1.14
15	75.855	65.33	1.16	10.590	9.33	1.13
16	86.304	75.00	1.15	11.287	10.00	1.13
17	97.422	85.33	1.14	11.982	10.67	1.12
18	109.207	96.33	1.13	12.675	11.33	1.12
19	121.660	108.00	1.13	13.367	12.00	1.11
20	134.781	120.33	1.12	14.058	12.67	1.11
21	148.570	133.33	1.11	14.747	13.33	1.11
22	163.027	147.00	1.11	15.435	14.00	1.10
23	178.151	161.33	1.10	16.123	14.67	1.10
24	193.943	176.33	1.10	16.809	15.33	1.10
25	210.402	192.00	1.10	17.495	16.00	1.09
26	227.529	208.33	1.09	18.180	16.67	1.09
27	245.323	225.33	1.09	18.865	17.33	1.09
28	263.785	243.00	1.09	19.548	18.00	1.09
29	282.914	261.33	1.08	20.232	18.67	1.08
30	302.710	280.33	1.08	20.914	19.33	1.08
31	323.173	300.00	1.08	21.596	20.00	1.08

Now consider the situation represented in Figure 1 below.

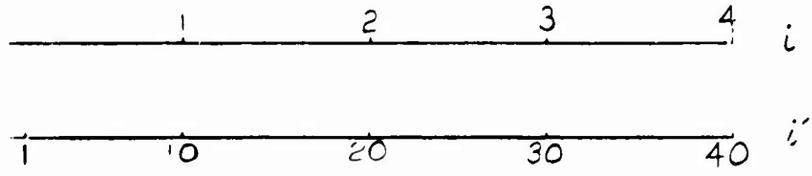

Fig. 1

The top line represents the state space with step size 1 and H = 4. If we take $\lambda = 1$ we find from Table 1 that $E(T_{14}) = 5.101$ for Case I'. The bottom line represents a state space with $\Delta = 1/10$. It is believed that sliding the first state to the left as shown is consistent with the approach taken in the usual continuous model. For the new state space we have (since $\lambda=1$) $\lambda'_{i'} = 100$. The first passage time which we want to compare is that from 1 to 30 on the new space. From Table 1 we find $E(T_{130}) = 302.710/100 = 3.027$. This is less than the value for step size 1 which is consistent with the fact that the continuous model gives shorter first passage times, and it is quite close to the value of 3.000 given by the continuous model. The above calculations for Case II' give $E(T_{14}) = 2.652$ for step size 1 and $E(T_{130}) = 20.914/10 = 2.091$ for step size 1/10. Again the change is in the expected direction and the continuous model gives 2.000.

It may be of interest to derive an approximate closed form expression for $E(T_{1H})$ in Cases I' and II' with $\lambda = 1$ and $\Delta = 1$. In other words we would like a closed expression for

$$\sum_{i=1}^{H-1} E(A_i)$$

where $E(A_i)$ is given by (15) with $\lambda = 1$. By the Euler-Maclaurin sum formula (Cramer [1], p. 123)

$$\sum_{\nu=1}^{i} \nu^{1/2} = \int_1^i x^{1/2}\,dx + \frac{1}{2} + \frac{1}{2}\,i^{1/2} - \frac{1}{2}\int_1^i P_1(x)x^{-1/2}\,dx$$

where $P_1(x) = [x] - x + \frac{1}{2}$ and $[x]$ is the largest integer not larger than x. Now $P_1(x) \leq \frac{1}{2}$ so

$$\int_1^i P_1(x)x^{-1/2}dx \leq \int_1^i \frac{1}{2}\,x^{-1/2}\,dx$$

$$= i^{1/2} - 1$$

and therefore

$$\sum_{\nu=1}^{i} \nu^{1/2} \geq \int_1^i x^{1/2}\,dx + \frac{1}{2} + \frac{1}{2}\,i^{1/2} - \frac{1}{2}(i^{1/2}-1)$$

$$= \frac{2}{3}\,i^{2/3} - \frac{2}{3} + 1 > \frac{2}{3}\,i^{2/3}.$$

Thus for Case I' we have

$$E(T_{1H}) = \sum_{i=1}^{H-1} E(A_i) > \sum_{i=1}^{H-1} \frac{2}{3}\,i^{2/3}\,i^{-1/2} = \frac{H(H-1)}{3}$$

which is to be compared with the result $(H-1)^2/3$ obtained from the continuous model. For Case II',

$$E(T_{1H}) = \sum_{i=1}^{H-1} E(A_i) > \sum_{i=1}^{H-1} \frac{2}{3}\,i^{2/3}\,i^{-2/3} = \frac{2}{3}(H-1)$$

which is exactly the result obtained from the continuous model.

This approach could perhaps be used with a better estimate of $P_1(x)$ to give a more accurate expression for $E(T_{1H})$ than is obtained with the continuous model.

Continuous Approximations

It is well known that the path of a classical random walk, itself a step function, may often be usefully approximated by a continuous function. Under many circumstances, this results in simplicity, and such an approach has been used to discuss the present problem. We shall explain the approximation method commonly used in terms of our Case I above. In terms of that example we can proceed heuristically in a natural way.

Rather than pass immediately to the continuous function approximation, let us suppose that our original process steps are of unit size (as they are), and that we wish to pass to an equivalent process acting over energy states of step size Δ. The idea of such equivalence is as follows: suppose our original particle begins its random walk on the original energy states, i.e. on those differing by unity; here we disregard the boundaries. Then at time t after the walk begins its position will have a certain probability distribution: the expected distance from the starting point and the variance of the resulting distribution will be

$$E(D_1) = (\lambda - \mu)t$$

and

$$\mathrm{Var}(D_1) = (\lambda + \mu)t \qquad (16)$$

and if λt and μt are at all large then the distribution of D_1 tends to the Gaussian described by the above parameters. If, on the Δ scale, we start a walk from the same place, utilizing rate parameters $\bar{\lambda}$ and $\bar{\mu}$ respectively, we find for D_Δ, the displacement on the Δ scale

$$E(D_\Delta) = (\bar{\lambda} - \bar{\mu})\Delta t$$

and (17)

$$\mathrm{Var}(D_\Delta) = (\bar{\lambda} + \bar{\mu})\Delta^2 t .$$

Again D_Δ tends to the Gaussian form with the same parameters. We say that the D_Δ-process is equivalent to the D_1-process if the above two limiting Gaussian distributions are the same, or if

$$E(D_1) = E(D_\Delta)$$

$$\mathrm{Var}(D_1) = \mathrm{Var}(D_\Delta), \tag{18}$$

which implies that

$$\lambda - \mu = (\bar{\lambda} - \bar{\mu})\Delta$$

$$\lambda + \mu = (\bar{\lambda} + \bar{\mu})\Delta^2 , \tag{19}$$

so we can solve for $\bar{\lambda}$ and $\bar{\mu}$ to find

$$\bar{\lambda} = \frac{1}{2}\left[\frac{\lambda-\mu}{\Delta} + \frac{\lambda+\mu}{\Delta^2}\right]$$

$$\bar{\mu} = \frac{1}{2}\left[\frac{\mu-\lambda}{\Delta} + \frac{\lambda+\mu}{\Delta^2}\right] . \tag{20}$$

It is intuitively appealing that any probability question asked about equivalent processes should provide approximately equal answers -- particularly if both processes must operate "for a long time", for this allows the tendency towards the Gaussian limiting form to occur. Thus we

may expect that we can utilize processes on finer and finer step sizes to calculate first-passage times to a "high state" H, with better approximation as H increases. We are interested in this possibility because it is conventional, and often convenient, to pass to infinitesimal step sizes (let $\Delta \longrightarrow 0$), i.e. to replace the random walk by "diffusion" or Brownian motion. We are interested in the error in such an approximate procedure. Refer to the following figure, illustrating the original walk, and the new one:

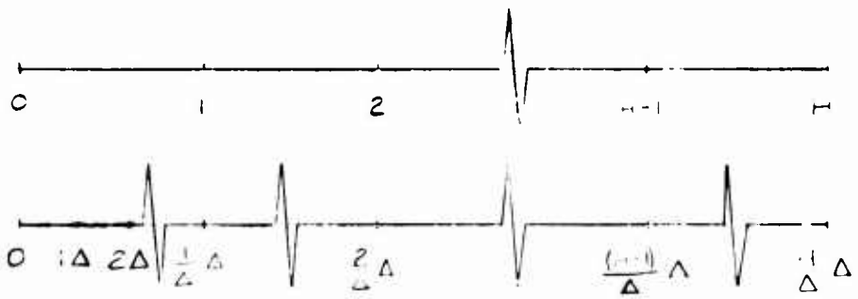

Fig. 2

Let us examine our Special Case I, translating to the new scale with step size Δ. Take Δ^{-1} to be an integer, so that we have an integral number of Δ-steps replacing one 1-step. Further let both walks start at the same place on the original scale: thus the new walk will start at $i = \Delta^{-1}$, for i on the new scale, and will end at $H\Delta^{-1}$. Then from (8) and (20) we get, for i on the new scale,

$$E(A_i) = \begin{cases} \dfrac{1}{\bar{\lambda}} \dfrac{1 - (\frac{\bar{\mu}}{\bar{\lambda}})^i}{1 - \frac{\bar{\mu}}{\bar{\lambda}}}, & \bar{\mu} \neq \bar{\lambda} \\ \dfrac{i}{\bar{\lambda}}, & \bar{\mu} = \bar{\lambda} \end{cases} \tag{21}$$

and

$$E(T_{1H}|\Delta) = \frac{1}{\bar{\lambda}-\bar{\mu}} \sum_{1=\Delta^{-1}}^{H\Delta^{-1}-1} \left\{1 - (\frac{\bar{\mu}}{\bar{\lambda}})^i\right\} = \frac{1}{\bar{\lambda}-\bar{\mu}} \left\{\frac{H-1}{\Delta} - (\frac{\bar{\mu}}{\bar{\lambda}})^{\Delta^{-1}} \left[\frac{1 - (\frac{\bar{\mu}}{\bar{\lambda}})^{(H-1)\Delta^{-1}}}{1 - \frac{\bar{\mu}}{\bar{\lambda}}}\right]\right\},$$

$$\bar{\lambda} \neq \bar{\mu}$$

$$= \frac{(H-1)(H-1-\Delta)}{2\bar{\lambda}\Delta^2}, \qquad \bar{\lambda} = \bar{\mu} \tag{22}$$

Now the appropriate scaling is given by (19) and (20). When we substitute for $\bar{\lambda}$ and $\bar{\mu}$ in terms of the original λ and μ a complicated expression results for <u>general</u> Δ. However, when $\Delta \longrightarrow 0$ a relatively simple limit results:

$$E(T_{1H}|0) = \frac{H-1}{\lambda-\mu} + \frac{1}{2}\frac{\lambda+\mu}{(\lambda-\mu)^2}\left[e^{-2(\frac{\lambda-\mu}{\lambda+\mu})H} - e^{-2(\frac{\lambda-\mu}{\lambda+\mu})}\right], \qquad \lambda \neq \mu,$$

$$= \frac{H^2-1}{2\lambda}, \qquad \lambda = \mu. \tag{23}$$

One can see that $E(T_{1H}|\Delta)$ <u>increases</u> for <u>decreasing</u> Δ when $\lambda = \mu$; this shows that <u>for this case</u> the continuous approximation <u>over-estimates</u> time of first passage to H. Although the comparison for different λ and μ can be made using (22), we have not done so here.

References

1. Cramer, H., "Mathematical Methods of Statistics", Princeton University Press, Princeton, 1946.

2. Feller, W., "An Introduction to Probability Theory and Its Applications", second edition, John Wiley and Sons Inc., N.Y., 1957, vol. 1.

3. Gaver, D.P. Jr., "Fluctuations Described by Birth and Death Process Probability Models", Westinghouse Scientific Paper 6-41210-2-P3, February 12, 1960.

Unclassified
Security Classification

DOCUMENT CONTROL DATA · R&D

(Security classification of title, body of abstract and indexing annotation must be entered when the overall report is classified)

1 ORIGINATING ACTIVITY (Corporate author) Westinghouse Corp Electronics Division Baltimore, Md	2a REPORT SECURITY CLASSIFICATION Unclassified 2b GROUP

3 REPORT TITLE

INVESTIGATION OF GAS IONIZATION PHENOMENON AT OPTICAL AND IR FREQUENCIES

4 DESCRIPTIVE NOTES (Type of report and inclusive dates)

Second Interim Progress Report, Feb - Dec 1964

5 AUTHOR(S) (Last name, first name, initial)

VanAllen, L.C. Gaver, D.P.
Wynant, R. Marshall, J.A.
Phelps, A.D.

6 REPORT DATE	7a TOTAL NO OF PAGES	7b NO OF REFS
February 1965	79	34

8a CONTRACT OR GRANT NO	9a ORIGINATOR'S REPORT NUMBER(S)
AF30(602)-3332 b PROJECT NO 5561 c Task No. 556106 d	9b OTHER REPORT NO(S) (Any other numbers that may be assigned this report) RADC-TR-64-568

10 AVAILABILITY/LIMITATION NOTICES

No limitation

11 SUPPLEMENTARY NOTES	12 SPONSORING MILITARY ACTIVITY
	RADC (EMASA) Griffiss AFB, NY 13442

13 ABSTRACT

The status of current work on Ruby Laser induced gas ionization is reported. Experimental measurements of the focused spot diameter, breakdown emission, ionization times and nonattenuation ionization are presented. The theoretical study results obtained to date in the areas of nonlinear ionization and the extension of microwave breakdown theory are discussed.

DD FORM 1 JAN 64 1473

Unclassified
Security Classification

Unclassified

Security Classification

14 KEY WORDS	LINK A		LINK B		LINK C	
	ROLE	WT	ROLE	WT	ROLE	WT
Ionization Lasers Plasmas Breakdown Argon Helium Air						

INSTRUCTIONS

1. ORIGINATING ACTIVITY: Enter the name and address of the contractor, subcontractor, grantee, Department of Defense activity or other organization *(corporate author)* issuing the report.

2a. REPORT SECURITY CLASSIFICATION: Enter the overall security classification of the report. Indicate whether "Restricted Data" is included. Marking is to be in accordance with appropriate security regulations.

2b. GROUP: Automatic downgrading is specified in DoD Directive 5200.10 and Armed Forces Industrial Manual. Enter the group number. Also, when applicable, show that optional markings have been used for Group 3 and Group 4 as authorized.

3. REPORT TITLE: Enter the complete report title in all capital letters. Titles in all cases should be unclassified. If a meaningful title cannot be selected without classification, show title classification in all capitals in parenthesis immediately following the title.

4. DESCRIPTIVE NOTES: If appropriate, enter the type of report, e.g., interim, progress, summary, annual, or final. Give the inclusive dates when a specific reporting period is covered.

5. AUTHOR(S): Enter the name(s) of author(s) as shown on or in the report. Enter last name, first name, middle initial. If military, show rank and branch of service. The name of the principal author is an absolute minimum requirement.

6. REPORT DATE: Enter the date of the report as day, month, year, or month, year. If more than one date appears on the report, use date of publication.

7a. TOTAL NUMBER OF PAGES: The total page count should follow normal pagination procedures, i.e., enter the number of pages containing information.

7b. NUMBER OF REFERENCES: Enter the total number of references cited in the report.

8a. CONTRACT OR GRANT NUMBER: If appropriate, enter the applicable number of the contract or grant under which the report was written.

8b, 8c, & 8d. PROJECT NUMBER: Enter the appropriate military department identification, such as project number, subproject number, system numbers, task number, etc.

9a. ORIGINATOR'S REPORT NUMBER(S): Enter the official report number by which the document will be identified and controlled by the originating activity. This number must be unique to this report.

9b. OTHER REPORT NUMBER(S): If the report has been assigned any other report numbers *(either by the originator or by the sponsor)*, also enter this number(s).

10. AVAILABILITY/LIMITATION NOTICES: Enter any limitations on further dissemination of the report, other than those imposed by security classification, using standard statements such as:

(1) "Qualified requesters may obtain copies of this report from DDC."

(2) "Foreign announcement and dissemination of this report by DDC is not authorized."

(3) "U. S. Government agencies may obtain copies of this report directly from DDC. Other qualified DDC users shall request through _____."

(4) "U. S. military agencies may obtain copies of this report directly from DDC. Other qualified users shall request through _____."

(5) "All distribution of this report is controlled. Qualified DDC users shall request through _____."

If the report has been furnished to the Office of Technical Services, Department of Commerce, for sale to the public, indicate this fact and enter the price, if known.

11. SUPPLEMENTARY NOTES: Use for additional explanatory notes.

12. SPONSORING MILITARY ACTIVITY: Enter the name of the departmental project office or laboratory sponsoring *(paying for)* the research and development. Include address.

13 ABSTRACT: Enter an abstract giving a brief and factual summary of the document indicative of the report, even though it may also appear elsewhere in the body of the technical report. If additional space is required, a continuation sheet shall be attached.

It is highly desirable that the abstract of classified reports be unclassified. Each paragraph of the abstract shall end with an indication of the military security classification of the information in the paragraph, represented as *(TS)*, *(S)*, *(C)*, or *(U)*.

There is no limitation on the length of the abstract. However, the suggested length is from 150 to 225 words.

14 KEY WORDS: Key words are technically meaningful terms or short phrases that characterize a report and may be used as index entries for cataloging the report. Key words must be selected so that no security classification is required. Identifiers, such as equipment model designation, trade name, military project code name, geographic location, may be used as key words but will be followed by an indication of technical context. The assignment of links, rules, and weights is optional.

Unclassified

Security Classification